A Device to Measure Tensile Forces in the Deep Fascia of the Human Abdominal Wall

Sponsored by Dr. Raymond Dunn of the University of Massachusetts Medical School

A Major Qualifying Report
Submitted to the Faculty
Of the
WORCESTER POLYTECHNIC INSTITUTE
In partial fulfillment of the requirements for the
Degree of Bachelor of Science
By

Olivia Doane

_____

Claudia Lee

_____

Meredith Saucier

_____

April 18, 2013

Advisor: Professor Kristen Billiar

_____

Co-Advisor: Dr. Raymond Dunn

_____

Table of Contents

Table of Figures

List of Tables

Authorship Page

The following paper was completed with equal contribution between all group members.

Acknowledgements

The team would like to thank the following individuals for their assistance throughout the progress of this project: Dr. Ronald Ignotz for assistance during animal testing, Lisa Wall for all her support, Alex Rangel for her contribution to the circuit construction, and Kevin Arruda and Greg Overton of the WPI machine shop for assistance with machining the final device.

Abstract

Ventral hernias have been found to occur in up to 25% of all midline abdominal laparotomy cases. In order to decrease the incidence of the development of ventral hernias, a relationship between tensile forces applied along the deep fascia and safety of closure needs to be established. To quantify the tensile forces in the deep fascia, a novel pair of hemostats was designed with hinged arms, rakes for attachment, and equipped with strain gages to be used in clinical studies.

Chapter 1: Introduction

The closure process for midline abdominal laparotomies, or vertical incisions through the linea alba of the abdominal wall, frequently results in complications and further damage to the surrounding tissues (Clark, 2001). This damage often causes ventral hernias, which are abnormal protrusions of tissue or an organ from its normal cavity along an incision site (Hernia, 2012) (Carriquiry, 1996).

During a laparotomy closure, the separated muscle pairs and deep fascia are first stapled shut (Cobb, 2005). The subcutaneous fascia, a continuous sheet of fibrous connective tissue, and the skin on both sides of the incision are then securely sutured (Stecco, 2011) (Cobb, 2005). If tensile forces applied to the wound during closure are too significant, the force exerted on the deep fascia can cause tissue ischemia, the restriction of blood flow to the tissue, ultimately resulting in the formation of a ventral hernia (Park, 2006). Up to 25% of all laparotomy cases result in the development of a ventral hernia (Hope, 2010).

In order to reduce the occurrence of a ventral hernia developing, it is essential that a relationship between tensile forces applied along the deep fascia and safety of closure be established. Currently, there is no definitive quantitative standard for the application of tensile forces, and the ability to safely close the incision is solely based on the surgeon's experience. The goal of this project was to contribute to the establishment of this relationship through the development of a novel medical device. The design consists of a modified pair of hemostats with hinged arms, rakes for attachment, and equipped with strain gages. It was successfully validated and tested for use in the operating room in future clinical trials. Application of this device in conjunction with the aforementioned relationship could allow surgeons to determine the optimal method for patient care.

Chapter 2: Literature Review

To completely understand the need, applications, and importance for the project scope, it is critical to establish a knowledge base in the areas of anatomy and laparotomies, closure methods and products, and current devices that are available to measure tensile forces.

2.1 Anatomy

The anatomy of the abdominal wall consists of the three primary layers of skin, fascia, and muscles, which together create a complex anatomical plane with many individual components. When examining the constituents of each layer, it is important to consider not only the physiology, but also the mechanical properties because every element contributes to overall abdominal structure and function. While the skin and musculature of the abdominal wall are well defined physiologically and mechanically, the mechanical properties of the fascia, specifically the deep layer, have not been as thoroughly characterized.

2.1.1 The Skin

As the largest organ in the human body, skin covers the entire exterior body surface, accounts for approximately eight percent of total body mass, and has a thickness that ranges from 1.5-4.0mm (Standring, 2008). A self-renewing surface and a barrier against microbes as well as mechanical forces, chemicals, osmosis, thermal damage , and UV radiation, skin is the most immediate layer of immune protection, barring not only potential threats but initiating immune responses (Standring, 2008)(Proksch, 2008). As a unit, skin is anisotropically structured consisting of micro-components collagen, elastic and nerve fibers, small blood vessels, and lymphatics (Kenedi, 1975).These elements of skin are interconnected into networks surrounded by interstitial fluid, forming highly fibrous tissues of elastin, keratin, and collagen, all of which allows for the viscoelastic behavior of the skin when loaded (Kenedi, 1975) (Lim, 2010) (Silver, 2001) (Dunn, 1983).

2.1.2 The Fascia

Beneath the skin, the human body is encased in a thick layer of fibro-adipose soft tissue known as the fascia. Essential for return of blood flow, dissipation of tension stresses, and movement, interaction, and coordination of limbs and muscles, the superficial, deep, and epimysium layers

(shown in Figure 2.1) of the fascia envelop muscles, nerves, and vessels (Stecco, 2011) (Findley, 2012) (Gallaudet, 2008). As a continuous sheet of fibrous connective tissue, the fascia swathes, separates, and binds together muscles, organs, and soft body structures, offering a layer of protection and transmitting up to 30% of muscle forces (Stecco, 2011).

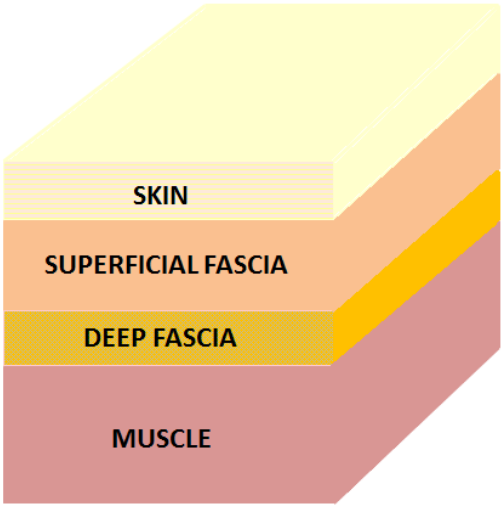

Figure 2.1: Illustration of the layers of the fascia.

The Superficial Fascia

Located directly underneath the skin is the superficial fascia, an uninterrupted subcutaneous layer of connective tissue containing a variable amount of fat in the form of large lobule-like deposits that are stacked between the lamellar, honeycomb structures of fibrous septa (Standring, 2008) (Stecco, 2011) (Gallaudet, 2008). The superficial fascia, which anchors the dermis to deeper layers, has a constant, well-defined macroscopic orientation perpendicular to the surface and is mechanically strong for both compression and tension loads (Stecco, 2011). Lying directly between the dermis and the deep, membranous fascia, the superficial fascia is a fibro-elastic tissue, dense and areolar in texture, consisting of a web of interwoven collagen fibers that are packed and mixed with abundant elastic fibers (Standring, 2008) (Stecco, 2011) (Findley, 2012).

The Deep Fascia

The deep fascia—a fibrous, membranous sheath responsible for shrouding and separating nerves and vessels, strengthening ligaments, and binding structures together into compact masses—has properties which vary from region to region throughout the body (Gallaudet, 2008). The thickness and strength of the fascia at each location corresponds to forces generated by the

surrounding muscles. Deep fascia is a connective membrane nearly devoid of fat, and is composed of autonomous fibrous planes that aid in muscle contractions (Stecco, 2011) (Findley, 2012). In the abdominal region, the deep fascia consists of thin layers of connective tissue of approximately 156μm that strongly adhere to the surrounding musculature. These layers physiologically mimic thin lamina of collagen fibers, but also contain an irregularly distributed mesh of elastic fibers and nerve fibers (Stecco, 2011) (Findley, 2012). The superficial and deep layers of the fascia are shown below in Figure 2.2.

Figure 2.2: A surgical incision showing superficial fascia and deep fascia (Carriquiry, 1996).

2.1.3 Biomechanics of the Fascia

As a continuous, viscoelastic matrix offering structural support and enveloping muscles, organs, and vessels, the fascia is essential for dissipating and transmitting mechanical forces between muscles. The consistency of the fascia changes according to mechanical loading, and exhibits different combinations of properties such as plasticity, elasticity, and malleability (Findley, 2012) (Kirilovam, 2009). Because the fascia is an incompressible biological tissue consisting of elastin in the fibers and numerous collagen bundles, it is able to maintain its volume before and after loading (Findley, 2012), and can act orthotropically (in the direction of loading). When the fascia becomes inflamed or swollen, it tightens and loses pliability (Kirilovam, 2009).

Minimal one-dimensional tensile testing of human abdominal fascia has been conducted in order to examine the viscoelasticity, non-linearity, and anisotropy of the tissue (Kirilovam, 2011). Samples of abdominal wall fascia were retrieved from deceased donors with no previous abdominal injuries and cut parallel and perpendicular to the direction of collagen fibers. Tensile testing was conducted at an elongation rate of 0.13mm/s with a maximum load of 500N (Kirilovam, 2011). Initial stress-strain curves showed that at a strain of 5%-7%, collagen fibers began to rupture, and a 4% strain rate was employed as a non-damaging rate for repeatable

loading and unloading tests (Kirilovam, 2011). Stress-strain curves generated at a 4% strain rate showed large variability between fascia samples, but all showed multiple peaks, indicating the uncrimping and stretching of collagenous bundles during loading. The viscoelasticity of abdominal wall fascia is further supported by the varied elastic moduli and ultimate tensile stresses (UTS): for samples cut parallel to collagenous fibers, the mean elastic moduli was 10.36±4.76MPa and the UTS was 1.61±0.46MPa; and for samples cut perpendicular to fibers, the mean elastic moduli was 3.3±2.12MPa and the UTS was 0.93±0.32MPa (Kirilovam, 2011). Parallel samples exhibit a greater elastic modulus and UTS primarily due to the mostly uniform orientation of the collagen fibers.

In the toe region of the stress-strain curves (see Figure 2.3), the viscoelastic nature of fascia is evident, a behavior which can be attributed to collagen fiber bundles located within the tissue. Under an applied stress, these bundles, which are most responsible for the mechanical aspects of the fascia, begin to loosen as sacrificial bonds between collagen molecules are easily broken. Microscopic examination showed that the structural components of collagen and elastin began to align in the direction of the applied load, and produced stress-strain graphs demonstrated a viscoelastic response (Song, 2004). This allows for some initial stretch in the tissue, a quantity that increases as the elastin begins to linear-elastically deform and collagen bundles continue to expand further until failure (Kirilovam, 2011).

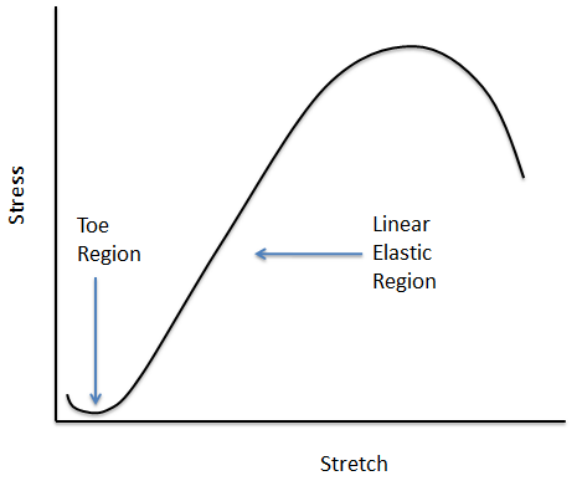

Figure 2.3: Characteristic graph showing typical regions for viscoelastic tissue.

A study of the biomechanics of the superficial fascia attempted to characterize properties of human abdominal tissue through tensile testing (Song, 2004). Samples were placed in a tension

meter, preloaded with 5N, and preconditioned between 0 and 13mm of elongation for 20 cycles at a rate of 50mm/min (Song, 2004). The superficial fascia was found to have a failure load of 102.6±74.4 N, and when the dermis and fascia were evaluated as a single unit, the value for failure load increased to 401.4±44.9N (Song, 2004).

The biomechanics of the combined superficial and deep fascia layers was examined for suture pullout force along the linea alba, the location of the incision made for midline abdominal laparotomies. Soft tissue was removed from the 346 test samples of fascia, and a single suture loop was placed in each section according to traditional suture technique for closure of laparotomy (Campbell, 1989). Sutures were then pulled out from the fascia, and data was collected corresponding to these forces. Data showed that the maximum force required for suture pullout was 58.2N (Campbell, 1989). While previous research has been able to gather mechanical data for yield strength and ultimate tensile strength, the data is greatly varied between studies, indicating a lack of a consensus about the mechanical properties of the fascia.

2.1.4 Muscles of the Abdomen

The anterolateral musculature of the abdominal wall consists of the rectus abdominis, the obliques, and transversus abdominis. As a unit, these muscles form the core, allowing for human bodily functions such as expiration and coughing; movements such as walking, bending, and flexing; and offer a layer of protection to organs (Standring, 2008).

The Rectus Abdominis, Rectus Sheath, & Linea Alba

The rectus abdominis (Figure 2.4) consists of two muscular bands encased in an aponeurotic, fibrous sheath on each side of the linea alba that stretch down the front of the abdomen approximately from the base of the sternum to the pubis (Standring, 2008) (Carriquiry, 1996). It is a long, flat, strap-like muscle transversely intersected three times by fibrous bands which fuse with fibers of the muscle sheath (Standring, 2008).

The surrounding rectus sheath (Figure 2.4), formed by fibers from the external and internal obliques and the transversus abdominis, encloses each portion of the rectus abdominis and is joined by the fascia and other connective tissues in the lower third. The combination of the rectus abdominis with the sheath can withstand up to 180N of force applied in a transverse direction,

and requires sutures that retain high tensile strength when surgeries are performed (Carriquiry, 1996).

Extending down the length of the abdomen between the pair of rectus abdominis is a tendinous raphe known as the linea alba (Figure 2.4). Formed by the interlacing and crisscrossing aponeurotic fibers of the external and internal obliques (which attach to the fascia) and the transversus abdominis, it is physically shown as a light groove in lean, muscular bodies (Standring, 2008) (Carriquiry, 1996).

The Transversus Abdominis

The deepest of the lateral abdominal muscles, the transversus abdominis runs perpendicular to the linea alba, wrapping around the sides of the abdomen and attaching to the twelfth rib and diaphragm. Lower fibers of the transversus abdominis curve downwards, extending to the inguinal ligament (Figure 2.4), while medial fibers decussate and blend with the linea alba (Standring, 2008).

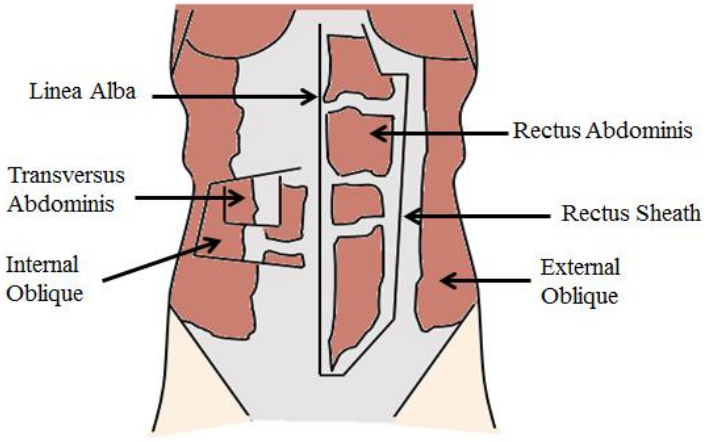

Figure 2.4: Diagram showing the different muscles of the abdominal wall.

2.2 Laparotomies

A laparotomy is any surgical incision into the abdominal wall or cavity, often performed on an exploratory basis, in order to identify the origins of pain or disease, or on a therapeutic basis, to treat and manage a previously identified medical problem (Carriquiry, 1996). A variety of incision types and their placement allow medical professionals access to the digestive tract; the liver, pancreas, gallbladder, and spleen; the bladder; female reproductive organs; the kidneys,

aorta, and abdominal lymph nodes; and the appendix (Pfannenstiel, 1990). Exploratory laparotomy is used to investigate the abdominal cavity and visualize the organs for diagnostic purposes. It is performed to determine the cause of symptoms and to establish the extent of a disease or illness (Carriquiry, 1996).

The procedure begins by placing the patient under general anesthesia so that the patient remains unconscious during the procedure, experiences no pain, has no memory of the procedure, and so that the muscles of the patient remain completely relaxed, allowing for safer surgery. For a midline laparotomy, an incision is made along the linea alba extending from the base of the ribs as far as the pubic bone. The incision, performed with a scalpel, begins by cutting through the skin and is then extended through the fascial layers and the abdominal muscles. In order to limit excess bleeding and for a more precise cut, electrocautery units are often used. Once the incision has been made retractors are attached to the skin and fascial layers and pulled back to better open the abdominal cavity (Laparotomy, exploratory 2007).

When doctors and surgeons have completed the procedure, the surgeon begins closure of the wound. Muscles are first stapled together, and then the skin and fascia layers are pulled together and sutured shut. Resorbable staples and non-resorbable or slowly resorbable sutures are used for the closure process, and gradually dissolve as the wound heals. Sutures are often multifilament (braided), and made of polypropylene, which secure the tissue during the 9 to 12 months of required time for healing (Ceydeli, 2005). Sutures are typically placed one centimeter from the fascia edge with one centimeter increments. Larger increments between sutures can be used to reduce the tensile forces over the entire length of the wound, which is critical for the prevention of tissue strangulation and ventral hernia development (Cobb, 2005).

2.2.1 Muscles and Fascia in Closure

Because the patient is anesthetized for the duration of the procedure, the muscles are completely relaxed and free movement is experienced. When the abdomen is intact, the muscles are extended in tension, allowing for muscle fibers to contract. Therefore, when the linea alba is cut, the connection between pairs of muscles is severed and the ability to retain the tension is lost, causing the muscles to retract to the sides of the abdomen. The viscoelastic mechanical properties of the subcutaneous fascia cause the retracted position to become the new relaxed

position. Upon closure, it is the fascia that hinders the ability to return to the original closed position, ultimately causing the high tensile forces in the tissue that result in ventral hernias.

2.3 Closure Methods & Complications

During healthy closure of abdominal incisions, the wound is closed properly using the aforementioned technique, and the patient goes on to live a healthy life. This occurs when there are minimal inflammatory responses in the abdominal cavity from the surgery, resulting in a normal closure. However, during surgeries when organs are shifted and irritated, excessive inflammation in the surrounding tissues frequently occurs. When the closure procedure begins it is more difficult to close the wound because of the larger area to enclose (Garfin, 1981). Complications can result immediately after the procedure, or after a period of time following the procedure.

2.3.1 Consequences of Abnormal Closures

There are two possible immediate consequences of abnormal closures where swelling occurs: tissue tearing and ischemia. Tissue tearing will occur if the maximum longitudinal tensile force of the fascial tissue is exceeded. As the tissue tears, there is excessive damage done to the patient resulting in scar tissue formation and less healthy tissue remains for the closure procedure. Therefore, the decreasing amount of tissue available for closure results in an increased chance of further complications to occur (Clark, 2001).

The second consequence is tissue ischemia, which is any reduction of blood flow to the tissue, resulting in decreased oxygen and nutrient supply to the tissue. Tissue ischemia can be recovered if the blood flow is restored to the tissue, however if this blood flow is not restored, it ultimately results in tissue death or necrosis. It can be caused by a sudden reduction (acute) or slowly decreasing (chronic) blood flow. There are several risk factors for ischemia that can contribute to its formation, including: vascular diseases, such as arteriosclerosis or hardening of the arteries; trauma; high blood pressure; heart problems; diabetes; tobacco use; high cholesterol; physical inactivity; stress; family history; and increasing age (Byeon, 2012).

2.3.2 Ventral Hernias

If the wound is closed too tightly, there is an increased buildup of pressure inside the abdominal cavity, which the abdominal wall counteracts. When this pressure exceeds the abdominal wall pressure, the weakest part of the abdominal wall ruptures and an abnormal protrusion, or a hernia, occurs through the incision, shown below in Figure 2.5. This abnormal protrusion along the incision is considered a ventral hernia (Park, 2006).

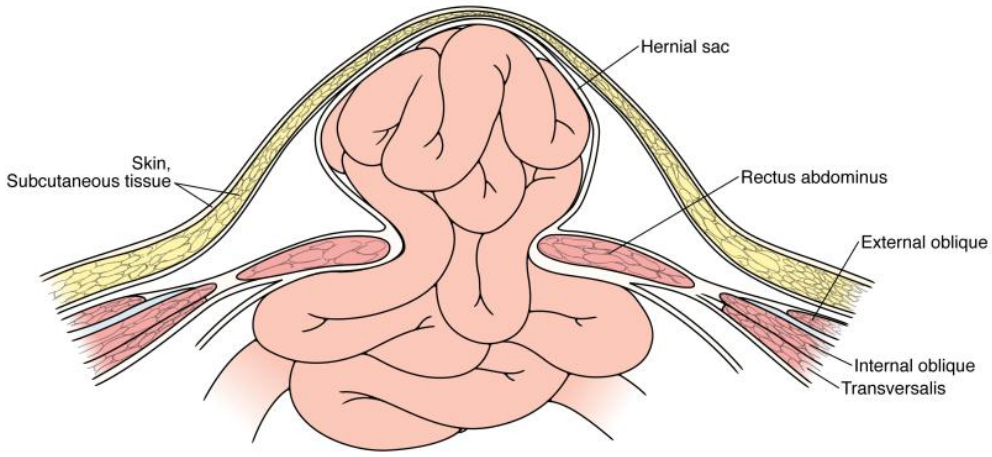

Figure 2.5 : Ventral Hernia formed along an abdominal incision (Lineaweaver, 2012).

A study conducted by Cobb et al. determined the pressures in the abdominal cavity during several routine activities. They found that during sitting and standing, pressures generated were 64 and 116 mmHg, respectively. Standing and coughing resulted in 141 mmHg, while jumping in place generated 252 mmHg. They concluded that the maximum tensile strength of an adult's abdominal wall to withstand routine activities is 27 N/cm. Therefore, if the pressure in the abdominal cavity was to exceed 27 N/cm, the abdominal wall would rupture, resulting in a ventral hernia (Park, 2006).

One in every five patients that undergo a laparotomy procedure develops a ventral hernia (Haroon, 2001). When ventral hernias are repaired, there is a recurrence rate of up to 50% depending on the surgical techniques used. It has been found that original ventral hernias can develop from three to five years after the surgery, while the recurrences have been found to occur within a year of the repair (Clark, 2001)(Haroon, 2001).

Symptomatic ventral hernias may range from minor discomfort to bowel obstruction and strangulation, although it is possible to have an anti-symptomatic ventral hernia (van Ramshorst,

2012). It is also possible that these hernias progress to become incarcerated, where the herniated tissue is trapped in a hernial sack. Both bowel strangulation and incarceration can lead to death. Incarceration is considered to occur in 10% of ventral hernias, and they have been found to commonly develop bowel obstruction and have a 50% occurrence of developing strangulated hernias. Twenty percent of strangulated hernias require intestinal resection. Mortality rates of incarcerated hernia repair are up to 5%, while for a strangulated hernia requiring bowel resection mortality rates are up to 20% (Park, 2006).

2.4 Temporary and Gradual Closures

There are a significant amount of products currently available related to the closure of the abdominal wall. These products and techniques used can be separated in terms of temporary abdominal closures (TAC) and gradual abdominal closures. For midline abdominal laparotomies, there are more techniques for preservation of an open abdomen that is necessary for repeated surgeries and gradual closure, than available devices and techniques used in normal uncomplicated surgeries.

2.4.1 Temporary Closures

Current products and techniques are available for use in the preservation of the open abdomen, which may be kept open for re-access and easy re-exploration, control of the abdominal contents, or the reduction of risk of intra-abdominal hypertension. In order to avoid the risk of a ventral hernia forming along the too tight incision closure, a graft, possibly an autograft of the patients' skin or polypropylene is applied over the open wound for protection (Kaplan, 2005).

A wide variety of materials are used for both absorbable and non-absorbable meshes. Absorbable materials include polyglactin 910 or polyglycolic acid, which are increasingly being used for TAC due to the reduced rate of intestinal fistulae that occurs (Schachtrupp, 2002). An intestinal fistula is the connection of the gastrointestinal tract and another epithelialized surface such as another organ (Stein). This compares to non-absorbable materials based on nylon, polypropylene, or polyethylene terephthalate which have a higher rate of fistulae of 4-75 %. The absorbable mesh also has a greater success rate from the ability to completely degrade after 6 weeks (Schachtrupp, 2002).

A study was conducted to compare the non-absorbable mesh material to absorbable mesh material. Here the fistula rate is much higher for polypropylene as well as the wound infection compared to the polyglactin. Overall, mesh has been a huge success in the preservation of the open abdomen in order to preserve the fascia with as minimal complications as possible (Schachtrupp, 2002).

Wittmann Patch is another example of an open abdominal technique that involves a Velcro material that is placed over the abdomen in addition to a mesh layer. Easy entrance through the Velcro patch allows for re-exploration and helps facilitate the closure of the abdomen, while continuous narrowing and trimming of the abdomen allows for eventual fascial closure. A problem seen with the Wittmann Patch is the high potential for Intra-Abdominal Hypertension (IAH) and abdominal compartment syndrome (ACS) (Kaplan, 2005).

While TAC techniques result in full patient recovery, aesthetically the incision healing is not up to par. After proper recovery, the patient returns to an entirely healthy state even without the physical closure of both sides of the abdominal wall. Possible methods are available that increase the closure time in order to reach a full and healthy fascial closure.

2.4.2 Gradual Closures

A common problem found in open abdomen cases is the retraction of the fascia. If the primary fascial closure is not completed within 7 to 10 days, the viscera will then adhere to the anterior abdominal wall (Stremitzer, 2004). At that point, the only option would be to allow the granulation of tissue to form over the abdominal contents over which a skin graft previously mentioned would be placed. To avoid this, gradual closure procedures currently in operation include the Bogotá Bag, and a vacuum assisted closure (VAC) in order to reach fascial closure. The problem with most of these techniques is that the closing process occurs over a period of a few days rather than of the time of the original surgery (Kaplan, 2005).

Bogotá Bag, named after Bogotá, Columbia, has been used since 1984 in the United States. The process consists of suturing a pre-gas-sterilized urology bag, or intravenous bag into the skin surrounding the incision to cover and maintain the abdomen. The reason for the popularity of this technique is from the readily available components, low cost, prevention of adherence of the viscera, and the ease of application (Kaplan, 2005). Although the Bogotá Bag has been used for

over 20 years, there is a wide range of drawbacks. Possible tearing of the skin at the attachment site, need for gas sterilization, difficulty in re-entry if deemed necessary, and the minimal control of third space available for the normal swelling of the viscera after closure leaves the Bogotá bag lacking efficacy. However, this technique has marked the start of development for new devices for the prevention and treatment of IAH and ACS regarding this initial idea and technique (Sukumar, 2004).

Vacuum assisted closure (VAC) or vacuum pack is one of the modifications that stemmed from the Bogotá Bag concept. This device allows for the prolonged closure of the abdominal wall through the application of wall suction, while simultaneously controlling abdominal secretions. The viscera are covered with a perforated, nonadherent polyethylene sheet followed by moist surgical towels. Next, two 10-inch French silicone drains are placed on the wound. An indoform-impregnated adhesive dressing is used as a sealant. A constant wall suction of 100-150 mmHg is applied. This method is both inexpensive and shows a high level of effectiveness (Kaplan, 2005).

VAC Therapy a modification of the previously described technique upon development was the only system verified by the Centers of Medicare & Medicaid Services for negative wound therapy. While the vacuum pack was successful in full fascial closure 9 days post-operatively, VAC Therapy was successful up to 49 days post-operatively. This technique uses reticulated polyurethane foam dressing to apply a subatmospheric pressure to the open abdomen. The foam that is used acts as suction cups along the wound applying the sub atmospheric pressure and also removing any fluids that arise, thereby stimulating cell growth. A computerized vacuum pump regulates the negative pressure applied to the wound surface. A pressure of 125 mmHg is the starting pressure, which was the critical pressure found to maximize cell reproduction. This method of abdominal closure demonstrates safety and efficiency in controlling the third space loss and closing the abdomen in a timelier manner although contact of the VAC foam with the bowel can result in fistula formation, therefore the process takes great level of precaution (Kaplan, 2005).

Sandwich Mesh Abdominal Closure (SMAC) is one modification in the management of an open abdomen through the combined application of mesh and the VAC process. The surgical technique used during this procedure is a staged abdominal repair (STAR) operation (Biswajit, 2004). This consists of re-entry into the abdomen every 24-48 hours, in order to achieve full

closure of the fascia. This SMAC uses a polypropylene mesh sutured to the fascia in order to prevent fascial retraction as well as preventing the formation of a ventral hernia by acting as a protective membrane over the viscera. Over time, the polypropylene mesh is cut longitudinally and drawn 2-3cm closer pulling the fascia closer. Over a repeated process of pulling the mesh tighter, fascial closure can eventually be reached. The SMAC VAC technique has been proven to be successful for treating patients with prolonged open abdomens (Hutan, 2010).

Table 2.1 compares the seven methods of closure, including temporary closure (Kaplan, 2005). For each method, the percentage of fascial closure and fistula occurrence is recorded. From the studies, VAC Therapy was found to be the most effective technique for abdominal closure. With the highest percent of fascial closure, 79 %, and the lowest fistula occurrence, 2.6 %, VAC Therapy has the best success rate. Polypropylene mesh and Polyglycolic mesh have very similar but lower fascial closure percentages, 33-34 % and a much higher percentage of fistula occurrences, 21-22 %. Mesh grafting was found to be least beneficial in maintaining an open abdomen.

Table 2.1: Comparison of fascial closure methods and fistula occurrence percentages (Kaplan, 2005).

Technique	Number of Cases	Fascial Closure N (%)	Fistula Occurrence N (%)
Polypropylene	175	44 (34)	28 (21)
Polyglycolic	667	129 (33)	87 (22)
Bogota Bag	553	48 (18)	35 (13)
Vacuum Pack Method	358	143 (58)	17 (7)
V.A.C. Therapy	327	181 (79)	6 (2.6)

Another gradual closure device that is currently in use is the DERMAClose® RC, a continuous external tissue expander that attaches to the skin and can be applied to assist in a prolonged closure of an open wound. Unique to this device is the large range of applications: in addition to the abdominal wound closures, DermaClose is also typically used in traumatic injuries, scar revision, excisional wounds, large skin deficits, skin cancer removal, and many others (DermaClose®RC).

Specific to the abdominal closure, brackets are securely stapled in the skin through which a nylon cable is wound through in a shoelace weave. The continuous nylon cable loop extends from the main body of the device, where it is connected to a ratchet. When the ratchet is tightened to the maximum setting, a consistent tensile force is applied to the brackets gradually reducing the size of the wound opening (DermaClose®RC).

While the DermaClose has had a great deal of success stories, they are limited to the closure of the skin for applied wound closures. The device has not been as useful for abdominal wound closures because the brackets are only attached to the skin and not the fascia where there is high resistance to closure. Another problem with this device is the inability to adjust the constant tension that is being applied (DermaClose®RC).

2.5 Gap in Research

The biggest area of research that is missing is regarding the applied tensile forces for the closure of the deep fascia. While there may be successful surgical techniques and products for wound closure, the lack of a safe tensile force being applied to the deep fascia can still lead to the formation of a ventral hernia. With all the current products and techniques available for closure, theoretically there should be a smaller percentage of abdominal laparotomy cases resulting in the formation of a ventral hernia. In order to increase the number of patients with a healthy normal recovery, a quantitative standard of safe tensile forces the deep fascia is able to withstand needs to be determined. Without this standard, the incidence of ventral hernias amongst laparotomy patients will remain at 20% and could potentially increase.

2.6 Current Devices for Tensile Force Measurements

Presently there are no devices that exist that are capable of attaching to the fascia in order to apply and measure a tensile force. A patent search was conducted in order to determine current solutions and their different characteristics that are effective or non-effective for clinical applications.

A skin transplant tension measuring apparatus is used for testing the tensile stress upon surgical transplantation of skin grafts. The design consists of pincer or forceps-like device that has two clamping legs connected together to form a gripping part. At this vertex there is a tensiometer,

which would measure the skin tension occurring during the implantation procedure to avoid tearing sutures (Breger, 1984). A drawing of the design can be seen in Figure 2.6 below. Although this device accomplishes a similar goal, the device would not properly suit the necessary characteristics of attachment to the fascia.

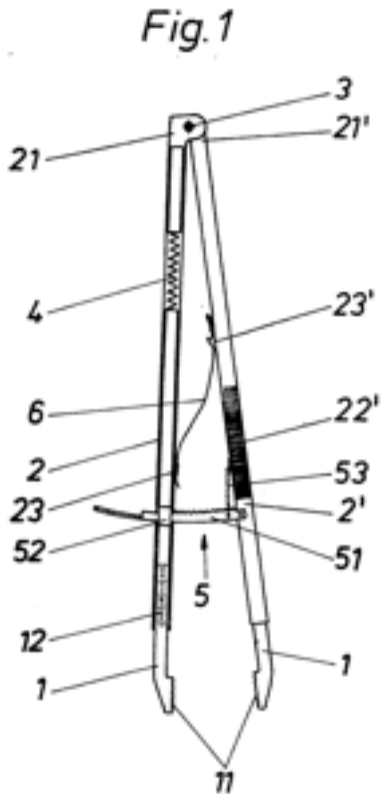

Figure 2.6: Schematics of skin transplant patent design (Breger, 1984).

A more relevant design is a patent on a forceps system that includes the measurement of signals indicative of the compressive and traction forces exerted by the forceps when in use. A micro-electromechanical piezoresistive force sensor is located in one of the forceps' members, and a strain gage is mounted on the external cylindrical surface. Forceps are commonly used to grasp tissue in surgical applications, and this device is geared towards finding the compressive forces exerted on the tissue (Harper, 2011). A schematic of the patent can be seen in Figure 2.7. Clamps are commonly used on vascular surfaces to provide stabilization however must be removed quickly after the procedure is finished to avoid a tourniquet effect (Fox, 2009). Through the use of hooks, an atraumatic effect is experienced reducing the chance of diminishing the blood flow to the targeted region.

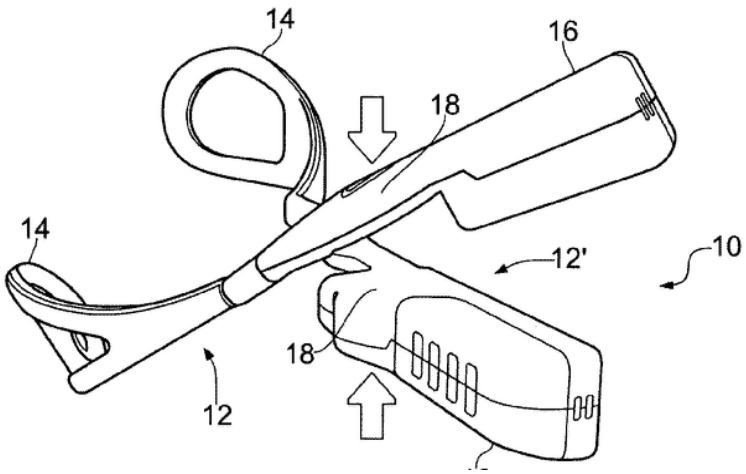

Figure 2.7: Schematic of compressive and traction forceps (Harper, 2011)

A similar patent for forceps also measures the force that is applied in the jaws of the device through the use of a force sensor, which is shown in Figure 2.8. On the outward facing surface of each forceps' member, there is a proximal portion of the arm extending over the force sensor. When a force is applied on the inward facing side of the jaw, the extended arm engages the electronic force sensor. The device was designed in order to assist in determining quantitative tension measurements applied to pull tissue together for suturing and holding in place. This device would not be suitable in our application because the clamping jaw would not be able to grip the fascia without tearing or puncturing the underlying viscera (Muthu, 2011).

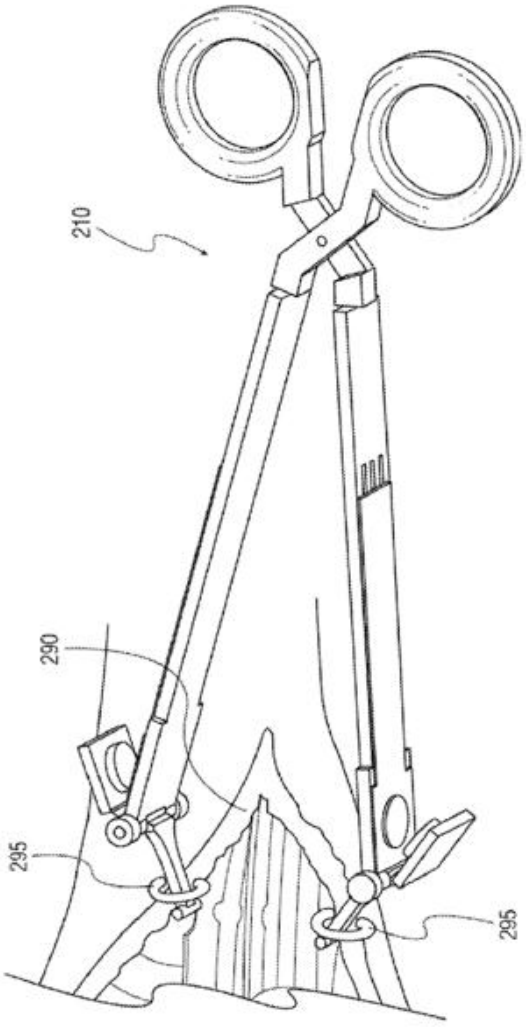

Figure 2.8: Schematic of various embodiments of the forceps design (Muthu, 2011)

Since current tensile force devices are not intentionally designed for use in the operating room, the sterility and safety regarding the location of the device within the open wound leave general measurement devices unsuitable. The attachment of the device to the fascia remains the largest hurdle because of the minimal thickness and proximity to the underlying viscera layer.

Chapter 3: Project Strategy

In order to successfully complete the project, a plan for all steps of the design process needed to be determined before moving forward. The overall validation of the project and the design needed to ensure timely results and thoughtful processes to determine the calculations necessary and the testing protocols for all tests conducted and data obtained. The approach to how the project was to be completed began with the initial client statement and ended with the data analysis and conclusions, including all the design steps in-between.

3.1 Initial Client Statement

To design and manufacture a device that easily, effectively, and safely measures tension at various points along the fascia of the abdominal wall. The finalized device will be applied to patients undergoing midline abdominal wall laparotomies. Data collected will be used to quantitatively define safe levels of tension for closure of abdominal incisions to prevent ventral hernias.

3.2 Objectives

After determining project goals, it was decided that easy to use, effective, safe, and manufacturability were the four overlying objectives for the device. A detailed objectives tree and pairwise comparison chart (PCC) completed by Dr. Raymond Dunn at UMass Medical School, PCC completed by the team, and a combined PCC can be found in Appendix A, B, and C respectively.

Easy to Use – It was crucial that the device is lightweight and portable for use by the surgeon as well as for effortless and manageable transfers between operating rooms. Simple data collection and wireless exporting to analysis software decreases the burden on the user. To achieve the most accurate data, the device must be easy to calibrate.

Effective – It was important that the device quickly attaches, applies tensile forces, measures, and records data in order to limit the time required for use of the device during surgery. The device must be reliable to ensure the collection of consistent and accurate data. In order to prevent damage and allow multiple uses, the device also should be durable.

Safe – It was critical that the device is sterilizable to avoid infection, damage, and additional harm to the patient. Since the resistance to closure in the fascia increases with time, data collection must be performed rapidly without compromising the accuracy or consistency of the data. Above all, the device must never harm the patient or user.

Manufacturable – Material choice is of the utmost importance because the device must be sterilizable to allow for initial application and reuse. It was important to keep cost at a minimum without compromising the quality of materials.

3.3 Constraints

Budget – The budget for this project is approximately $150 per group member, as provided by WPI. University of Massachusetts Medical School will be supplementing the budget as necessary throughout the project.

Time – The project must be completed by April 18, 2013.

Institutional Review Board/Institutional Animal Care and Use Committee (IRB/IACUC) – To perform testing on either human or animal subjects, it is essential that the IRB or IACUC approved the project, device, and experimental protocols prior to live specimen testing. Without these approvals, testing would not be conducted.

Patient Consent – If the IRB was passed, signed patient consent forms that fully disclose the nature of the testing would be required for every participant. Each patient would have the choice to participate in the testing of the device, and could opt out of the experiment at any time.

FDA Regulations & Restrictions – The FDA maintains strict rules and regulations governing what can and cannot be used for human testing. The potential for the device to be classified as unsafe for human testing beyond IRB standards would limit, if not eliminate, human testing.

Sterility – The device must be sterile before conducting any tests on a live subject to prevent the transmittance of bacteria or pathogens.

3.4 Revised Client Statement

To design and manufacture a device that measures localized tensile forces at various points along the deep fascia of the abdominal wall of patients undergoing midline abdominal laparotomies. The device will assist in closure while simultaneously recording the localized tensile force measurements that will assist in quantitatively defining optimal levels of tensile forces. This will ultimately allow surgeons to determine if immediate or gradual closure is preferred to prevent ventral hernias.

3.5 Project Approach

A set of functions and specifications were made in order to evaluate the possible means of accomplishing these tasks while following the goals from the objectives and limits due to constraints. A Functions-Means Chart was created to help create a completed list of the design elements. The next step was to generate design alternatives which had the potential to satisfy the project scope and compare these designs, ultimately choosing the best fit device. In order to overcome the limited budget for the project and achieve the objectives, it was necessary to generate designs based on maintenance of a strict list of materials and parts to be used. By selecting materials that were inexpensive yet sterilizable, the device can be reused and quickly manufactured, factors which both kept overall costs down. Proper selection of strain gages, wiring, and bulk materials ensured device functionality.

An essential component of the design process was device testing, a procedure that was limited by time, IRB/IACUC, and patient consent. Time as an overall constraint demanded thorough and highly detailed planning, and necessitated adhering to a tight schedule. Required IRB/IACUC paperwork for human and animal testing was completed and submitted for approval. Animal testing was conducted on swine cadavers provided by the University of Massachusetts Medical School. Testing of the device, which occurred in stages, consumed a bulk of total project time, and it was vital that the device be fully developed and ready for prototyping within the first fourteen weeks of design. In order to determine the amounts of strains the material was to experience, it was necessary to determine the amount of deflection that occurs at the maximum force that would be applied. Mechanical testing was to be completed to determine the deflection.

Completion of the initial prototype allowed for swine testing to be performed, and design modifications to be made to the retaining forceps. The re-design of testing protocols to achievable, more realistic procedures and refinements to design elements of the hemostats allowed for collection of a specific range of data. The verification data collected from the preliminary testing in animals had the potential to allow for progression to final testing.

3.6 Testing Protocols

Swine testing was conducted to confirm the approximate force needed for complete closure and also to verify the functionality of the final design. Sacrificed adult swine were provided for the study by UMMMS who at the time were performing their own swine studies. Each group member, to ensure proper knowledge of animal care and technique, completed an animal subject training and received necessary vaccinations.

3.6.1 Swine Weight Testing

The first test was used to determine the forces that are applied to the deep fascia of the swine. The swine cadaver was placed on its back, securing the legs apart and exposing the underlying abdomen. The first step was to mimic a midline abdominal laparotomy by creating an incision down the linea alba from the base of the ribs to the top of the pelvic region. Next, a small slit was made on one side of the incision, 1cm from the edge and a second slit was mirrored on the opposite side of the incision also 1cm from the edge. This allowed for the hooks on the ends of fish scale weights to be fed through. Pulling each weight across the wound, the abdominal wall was pulled to closure and the pound force that was applied was recorded. This was repeated at a few locations along the length of the incision to aid in gaging the approximate force that would be necessary for closure.

It was hypothesized that the middle point along the curve would require the greatest force because the fascia has retracted the furthest distance from the centerline of the incision. Respectively, we expected that both ends of the wound would need the smallest amount of force to reach the centerline. The measured forces were predicted to form a bell curve with the highest forces at the center.

3.6.2 Swine Prototype Testing

The second set of swine testing that was completed was the verification of our prototype including proof of concept for several design modifications. The overall functionality and ease of use of the design and the attachment to the fascia were tested and a sample set of data was recorded. Positioning the swine on its back and securing the swine prevented unwanted movements. A midline abdominal laparotomy was conducted, separating the muscle groups and fascia and exposing the viscera. Allowing time for the effects of the residual stress to occur on the deep fascia, the closure procedure was prolonged. Attachment to the deep fascia occurred at 1cm increments starting at either end of the wound and the application of the device was examined. At the completion of this testing, any necessary design modifications were made in order to better achieve the project goal.

Chapter 4: Design Alternatives

The functions and specifications for the design were established in order to set a standard of characteristics that must be achieved, and criteria by which the design had to abide. Initial design alternatives were created based on the original project goal to measure one overall tensile force distributed across the length of the wound. A second round of design alternatives were generated with the goal of measuring localized tensile forces. A final selection matrix helped to identify the ideal solution, resulting in the development of the final design. A set of protocols were written to obtain preliminary data for the feasibility of the design.

4.1 Needs Analysis

After thoroughly discussing with the client, the focus of the project was narrowed to satisfy exactly what was needed and what would be feasible. The key features of the device and design constraints were identified to solidify the project scope. The client asked for a device to measure tensile forces in the deep fascia of the abdominal wall while assisting in wound closure. In order to establish the most important design aspects, a pairwise comparison chart (PCC) was developed and completed by Dr. Dunn (shown in Appendix A) ranking which objectives were more important.

For functional needs, safety was ranked as the most important overall objective of the design. The device needed to be safe for both the patient and the user to reduce potential risks in the operating room. It was also necessary for the device to be sterilizable, either by using an autoclave or ethylene oxide gas. Accurate, reliable, and consistent were all ranked highly. It was necessary for the device to measure a maximum force required for failure of fascia tissue because the device must not damage the tissue.

When considering physical needs, Dr. Dunn rated portability as most important for the overlying objective of ease of use. The device needed to be highly portable and lightweight to allow for transfer between operating rooms. Although there were no major size limitations on the device despite the weight, the team discussed what size would be feasible for the device. Incision size varies between 4-10 inches in length and significantly in width; therefore the device must be able to accommodate up to the largest incision size.

4.2 Functions and Specifications

Once the team determined the detailed objectives, it was necessary to establish a list of essential functions the device must be able to perform. A general compilation of functions were further broken down into possible means for achievement. A Function-Means Chart was developed to organize the potential design basis, initiating the brainstorming process that guided the development of design alternatives.

4.2.1 Functions

The device needed to perform four major tasks: at various points along the incision, it must attach and detach to the deep fascia atraumatically; apply and measure a tensile force at each attachment site; provide accurate and precise data; and in order to account for a range of sizes amongst patients and laparotomy incision sizes, must be adaptable and adjustable.

4.2.2 Specifications

While the specifications for the device did not have any standard benchmarks, in order to achieve the objectives of lightweight and portable, it was determined that the device should not weigh more than .45kg (1lb), and should have the capacity to include a range of widths from 20mm to 80mm. Previous studies have shown that the mechanical properties of the abdominal wall vary and are dependent upon site, loading, and localized structure (Standring, 2008). One study examining the biomechanical properties of human fascia determined that the pullout strength of the fascia was 58.2 Newtons (N) (Campbell, 1989). Using this data as a quantitative limit on the tensile strength of the fascia, the device should not apply more than 58.2 N at each point of attachment with a tolerance range within 1%. Counteractive to this force, the minimal human grip force that can be applied is 68.1 N, and therefore any design would need to accommodate this grip strength (Mathiowetz, 1985).

4.2.3 Functions and Means

In order to determine potential methods for achieving the functions, a Functions-Means Chart was generated. Table 4.1 lists the functions of the device and possible means to achieve each.

Table 4.1: Functions and their corresponding means.

Function	Means					
Applies tensile forces	Hydraulic	Electromechanical	Mechanical	Hand	Drill	
Measures tensile forces	Gage	Transducer	Tension Meter			
Attaches to the fascia	Hook	Clamp	Tissue Velcro	Suture	Staples	Bracket
Adaptable/Adjustable	Retractable cables	Pivot Points				

Mechanisms for applying a tensile force include hydraulic systems, electromechanical designs, purely mechanical arrangements, manual, and power tools. Hydraulic systems involving pistons and engines may be too large and over complicate the design. Electromechanical options, such as a small motor, add an ease of use element to the design but risk uncontrolled over application of a tensile force. Purely mechanical applications of the device, such as a small hand crank, allow for user-applied tensile forces and allow the surgeon to limit the tensile force applied at each attachment site. However, this can be obtrusive and lack overall control because of the variety in the pull, the direction of the pull, and the steadiness of the pull. Power tools, such as a drill with a custom bit, allow for quick and easy application of tensile force at each site, and would require the close attention of the user to prevent excessive tensile forces. There are limits on how precise the application of the force could be because of the inability to make very small adjustments using a hand drill.

Measuring tensile forces demands that the device have a strain gage, torque sensor, force sensor, force transducer, or tension meter incorporated into the design, and may require the use of data collection software or virtual instrumentation such as LabVIEW. Strain gages would offer accurate data depending on the model and precision of the instrument, but do require an output to report data. Torque sensors, force sensors, force transducers, and tension meters are expensive options for measuring tensile forces, but offer an overall level of precise data collection comparable to strain gages.

Methods for attachment include suture loops, staples, brackets, hooks, clamps, and tissue Velcro. For the adaptable and adjustable function, retractable cables and pivot points were the possible

means for the design. Since these means could further be broken down, the team created another Functions-Means chart specific to these functions. This can be found in Table 4.2.

Table 4.2: A list of the two adaptable/adjustable functions and possible means.

Function	**Means**			
Retractable Cables	Spinning to coil	Spring & Ratchet		
Pivot Points	Cup & Socket	Rotating Tube	Track	Outside

The adaptable and adjustable function can be accomplished by introducing pivot points and cables at a length which can be pulled, attached, and retracted to accommodate a range of sizes. Pivot points could be designed to look like a cup and socket, where the cup could rotate in the socket and direct a cable in the appropriate direction. Encasing cables within a tube and moving the tube along a track and rotating it in the proper direction also allows the device to adapt along incisions of a wide range. Retractable cables could be designed using a compression spring and ratchet system commonly used in seatbelts and telescoping cables in hair dryers and vacuum cleaners. These cables could also be manually wound using a hand crank and stored in the body of the device.

4.3 Design Alternatives

The process through which design alternatives were created included multiple reevaluations and brainstorming in order to satisfy the needs established by the client. The first set of design alternatives was created with the intent to assist in closure of an abdominal laparotomy while measuring the single tensile force acting along the entire length of the incision. After further discussion with the client, it was determined that these designs did not fulfill all the goals of the project, and therefore a second round of design alternatives was conducted. The designs from round one can be found in Appendix E to K. The second group of design alternatives focused on measuring the localized tensile forces at various points along the incision. The design concepts that were developed are discussed further in the following sections. Once these were completed, a weighted functions-means chart was used in the selection process for the final design based on the second group of alternative designs.

4.3.1 Design 1: L-Shaped Handle Clamp

The L-Shaped Handle Clamp consists of a vertical section that would act as a handle, and an elongated section to attach to the deep fascia (shown in Figure 4.1). The clamp that would be attaching to the fascia and dermal layers would be lined with a set of moderately dull teeth, allowing for a greater contact area. Using a butterfly nut, the clamp would be tightened to the optimal fit. The user would apply the pressure using the force from pulling on the handle. In the top section of the clamp, a force transducer would be located in order to read the measured tensile forces, and would export data.

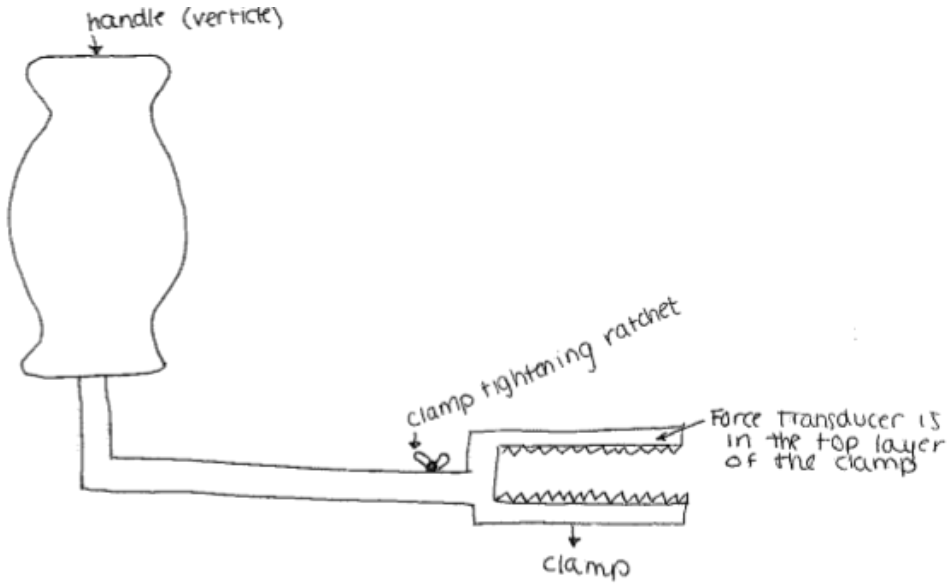

Figure 4.1: L-Shaped Clamp sketch

4.3.2 Design 2: Force Sensor

The first iteration of this design consists of a two-way force transducer measurement device, as shown in Figure 4.2 below. The device would have two cables attached to a spring that lead to force transducers. Cables would exit from the center of the body of the device, and could be locked in place via an anchoring mechanism or used for measurements. One cable would be used at a time, keeping the body of the device in the center, and the average of the two measurements could be taken. Data would be collected with the use of a force transducer located at the center of the device, and exported for analysis.

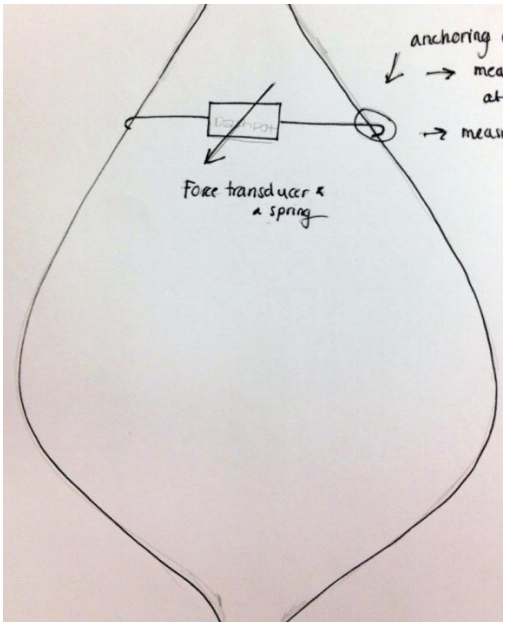

Figure 4.2: Force Sensor Iteration 1 Sketch

The second model of the design consists of a fixed center bar where multiple cables attached to springs and force transducers are attached (seen in Figure 4.3). There would be multiple cables along the length of the incision, all with individual attachment and measurement recordings. The multiple cables are attached to the center bar to ensure placement along the centerline of the incision.

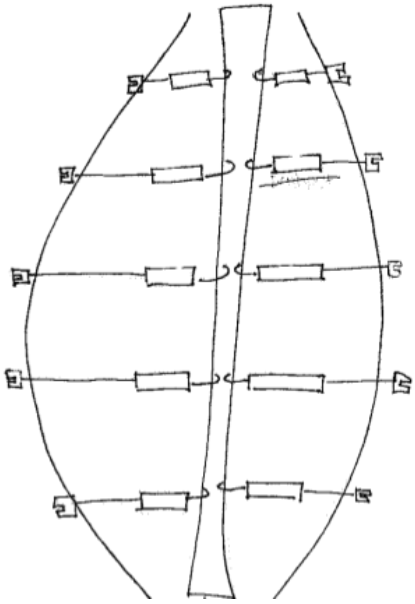

Figure 4.3: Force Sensor Iteration 2 Sketch

4.3.3 Design 3: Instrumented Forceps and Hemostats Variations

Forceps and hemostats are commonly used surgical tools that surgeons are familiar with. Modifying these tools through the attachment mechanism and the addition of a force measuring device would ensure ease of use. Six variations of designs were modeled based on different types of forceps and hemostats that are used. In general, when the tissue is gripped between the two pinchers and pulled, the force measuring device will output data correlating to the amount of tensile forces being applied to the deep fascia.

Variation 1

One option for modification of forceps focuses on altering the portion of Kelly forceps that will hold the tissue, as shown in Figure 4.4. These would be designed to be large, flat, solid, round pads: the force transducer would be located within the center of one of the pads and surrounded by small raised teeth; the opposite side would have small raised teeth along its outside edges; when the pads are squeezed together, the tissue would be grasped by the teeth and data would be transferred by the force transducer for data analysis.

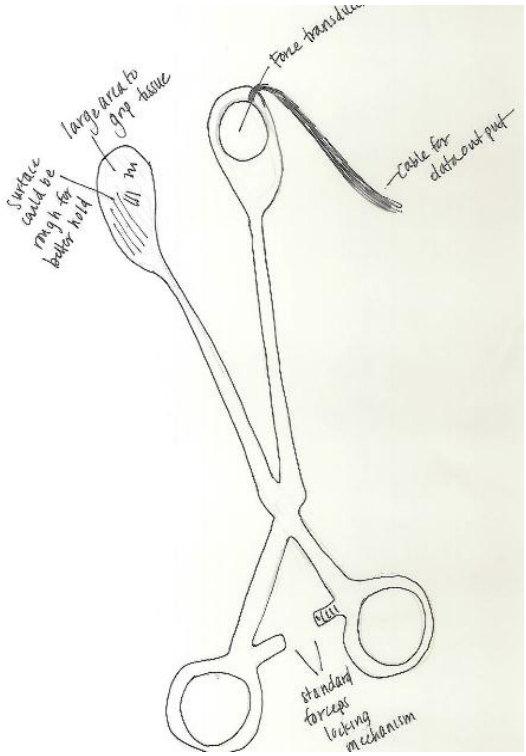

Figure 4.4: Kelly Forceps Design Modification with Pad Attachments

An additional method of instrumenting forceps begins by modifying a basic pair of Kelly forceps. The traditional attachment portion of the forceps would be altered to resemble rakes with a set of outward facing teeth that curved down, as shown in Figure 4.5. The teeth would grip onto the deep fascia, a locking mechanism near the handle would hold the tissue in place, and a force sensor located in the underside of the attachment bed would collect data. The forceps would also have an extended body so the handles could be moved away from the suturing site and not inhibit the closure process.

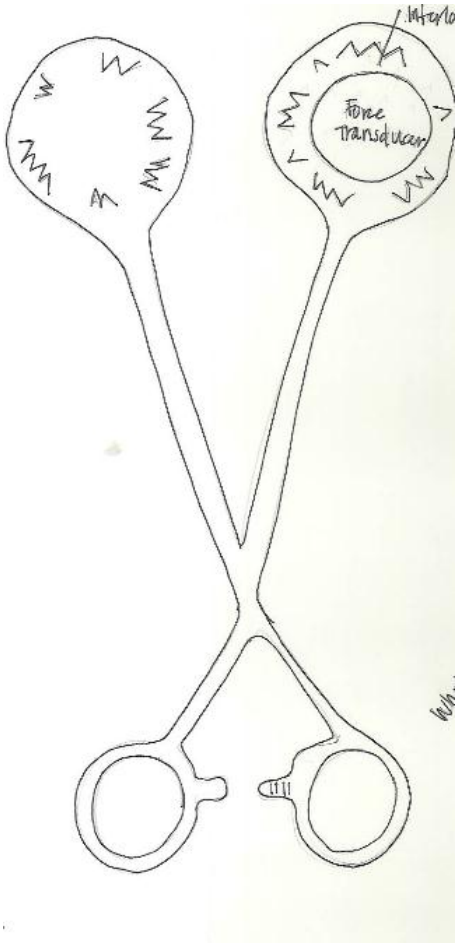

Figure 4.5: Kelly Forceps Modification with Teeth Attachment

Variation 2

A second option is to alter blunt nosed thumb forceps that resemble long, extended flat tweezers seen in Figure 4.6. A force transducer would be bonded to one inside pad of the forceps and would transmit data as the tissue is first squeezed and then pulled. For an immediate visual

output, a basic needle gage could be added to the body of the device and connected to the force transducer. As the tissue is pulled, surgeons would be able to easily watch the applied tension level and ensure that the tensile force is not excessive or causes damage to the tissue.

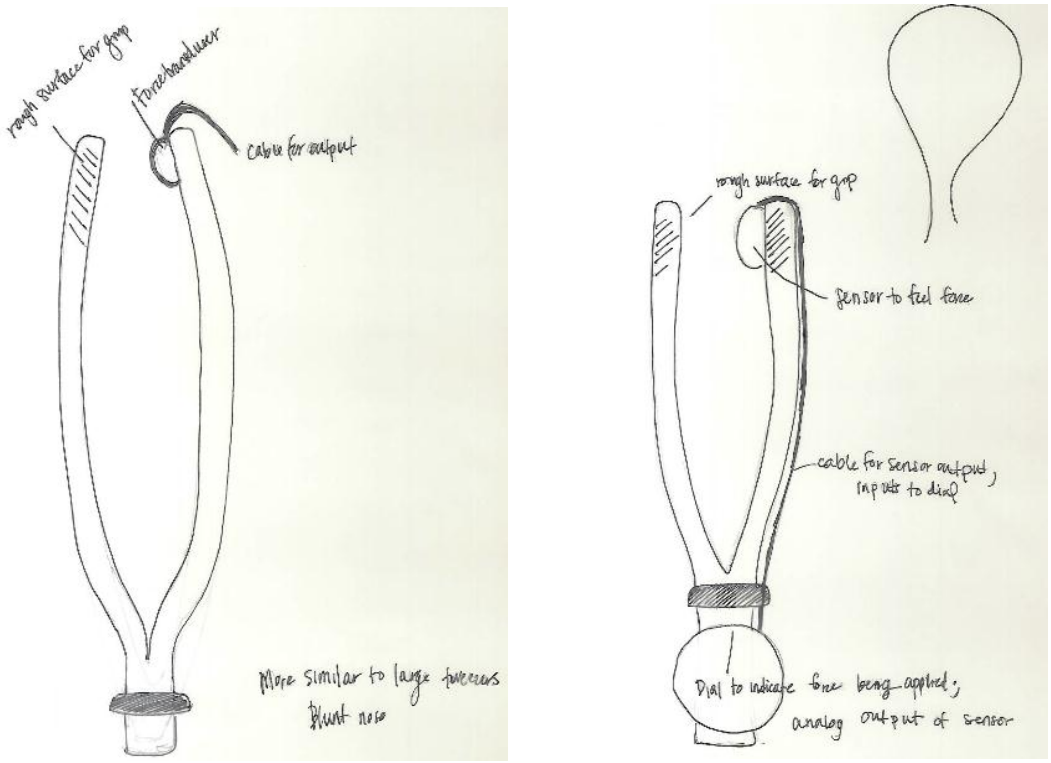

Figure 4.6: Modified Blunt Nose Thumb Forceps: left-tweezers attachment, right-pad attachment.

Variation 3

Forceps could be adapted to resemble a spatula at the attachment with multiple prongs branching out from a stem and interconnected at their ends, as shown in Figure 4.7. Each prong, with a roughened surface for improved grip, would grasp the tissue. After which, a force transducer located in one of the arms of the forceps would send data to a computer for further analysis.

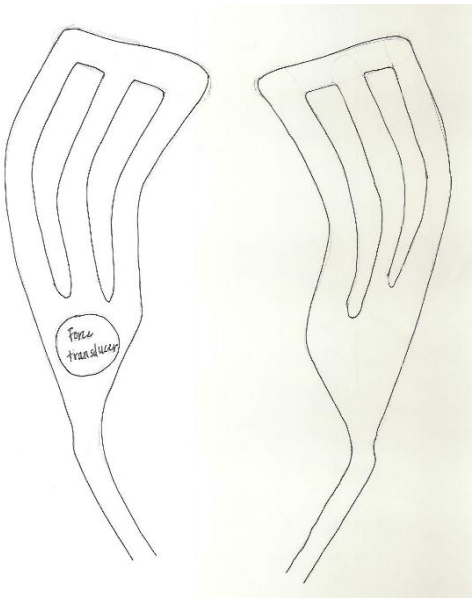

Figure 4.7: Forceps modification with Spatula Attachment.

Variation 4

Curved forceps, shown in Figure 4.8, are designed to roll inward when squeezed and firmly grasp the tissue with a set of blunt teeth. The deep fascia would then be locked in the forceps and pulled, applying a tensile force to be measured by a force transducer located in the end of one side of the forceps. Data would then be exported for analysis.

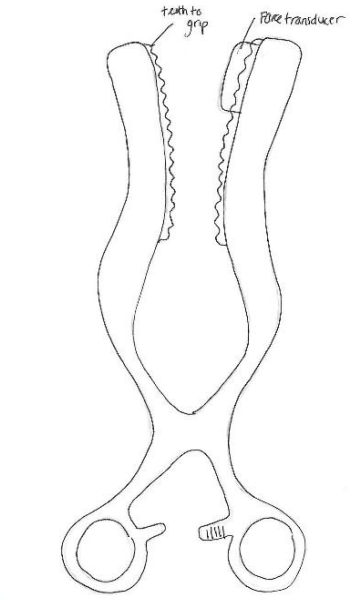

Figure 4.8: Instrumented Curved Forceps

Variation 5

Another design alternative for the standard forceps is the disengaging forceps, which primarily have the ability to separate into two separate pieces allowing for easier attachment and detachment to the deep fascia. The forceps, shown in Figure 4.9, would have a bent and elevated shape to accommodate the handles being kept from interfering with suturing. Forceps would end in small hooks that provide the means for attachment. Once attached to the fascia, the two parts can be connected at the pivot point where the top part containing a small hole will slide on the bottom part containing the corresponding pin. The surgeon would be able to apply the tensile forces by squeezing the handles of the forceps together. A surface mounted strain gage would be located in between the two forceps parts in order to measure the corresponding tensile forces in the deep fascia. This data will be used to calculate the strain using calibration factors and is sent through the display that will be located on the extended handle of the forceps.

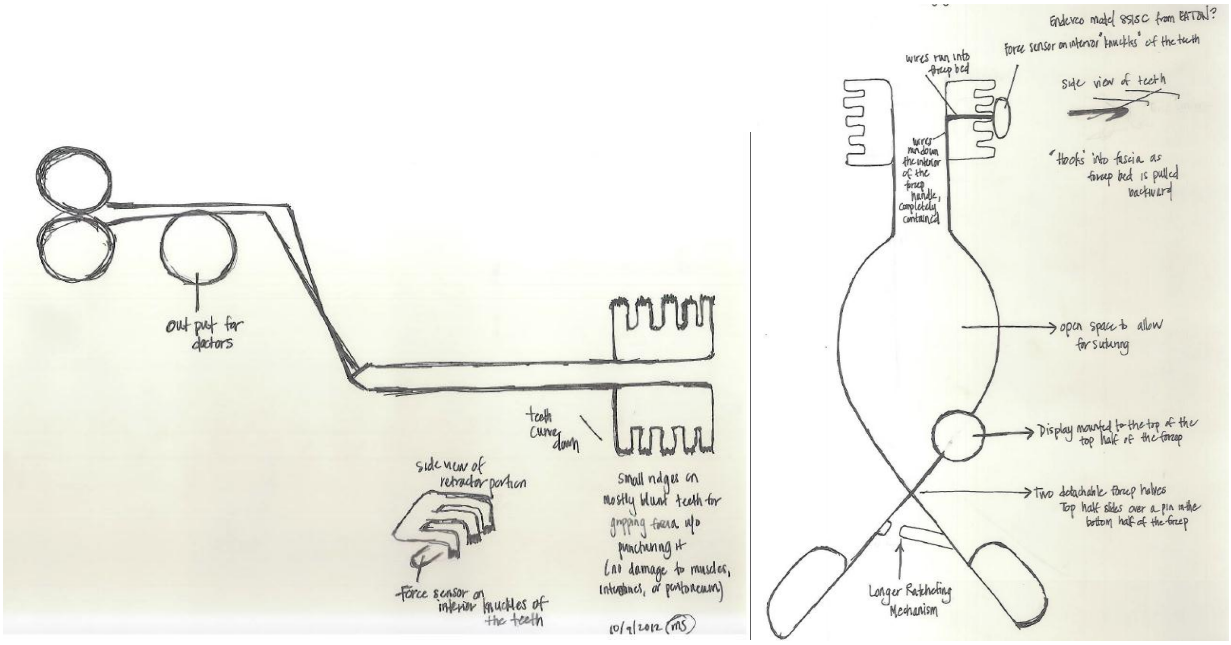

Figure 4.9: Disengaging Forceps Sketch: left-side view, right-top view

4.4 Final Selection Matrix

A selection matrix was completed in order to evaluate how well design alternatives met the objectives and constraints, as shown in Appendix L. Constraints were met by all second round design alternatives. Design objectives, which were weighted by importance according to the

combined pairwise comparison shown in Appendix D, were then numerically evaluated for each design. These totals were then normalized and compared (Table 4.3), and demonstrated that the Instrumented Kelly Forceps, Elevated Retractor Forceps, and Disengaging Forceps were the best device designs to meet the demands of the project. The Disengaging Forceps, which met all design constraints and had a normalized objectives score of 91.7/100, was selected as the final design.

Table 4.3: Selection matrix showing numerical evaluation of objectives for the top three designs.

Design Objectives		Instrumented Kelley Forceps		Elevated Retractor Forceps		Disengaging Forceps	
	Weight	Score	Weighted Score	Score	Weighted Score	Score	Weighted Score
Easy to Use	0.80	9	7.2	10	8	9	7.2
Effective	2.50	6	15	7	17.5	9	22.5
Safe	5.00	7	35	9	45	9	45
Manufacturability	1.70	10	17	10	17	10	17
Total	10.00	32	74.2	36	87.5	37	91.7

4.5 Conceptual Design

The Disengaging Forceps are specially modified to aid the surgeon in measuring the tensile forces in the deep fascia during approximate closure of the incision while limiting interference during the suturing process. The body of the forceps, shown below in Figure 4.10, is designed to be two separate straight arms (disengaged) while attaching to the deep fascia. Once attached, they can be placed together and the surgeon can apply a force. The hinge located just after the pivot point allows the forceps to be maneuvered out of the way after the forceps have been locked into position as can be seen in Figure 4.10. This would allow the surgeon to keep the incision site as accessible as possible. To maintain the straight position during attachment and application of force, a sliding lock was designed, which can be seen in the model below. In the pieces extruded upwards from the forceps body with the cut inside, a sliding pin would slide across when the surgeon decides to lock the forceps straight, blocking the hinge from movement. When the surgeon is ready to move the forceps out of the way and bend them downward, the sliding lock can simply be slid backwards and the hinge is released for free movement.

The forceps bed contains two micro-hooks (seen in the inset in Figure 4.10) that attach to the deep fascia without puncturing through the underlying peritoneum. To ensure a constant parallel

attachment to the deep fascia, the forceps' beds were designed to rotate left to right on a pin. A strain gage is bonded to one of the arms of the forceps and as the tissue is pulled, the strain measurements are converted into forces and numerically displayed.

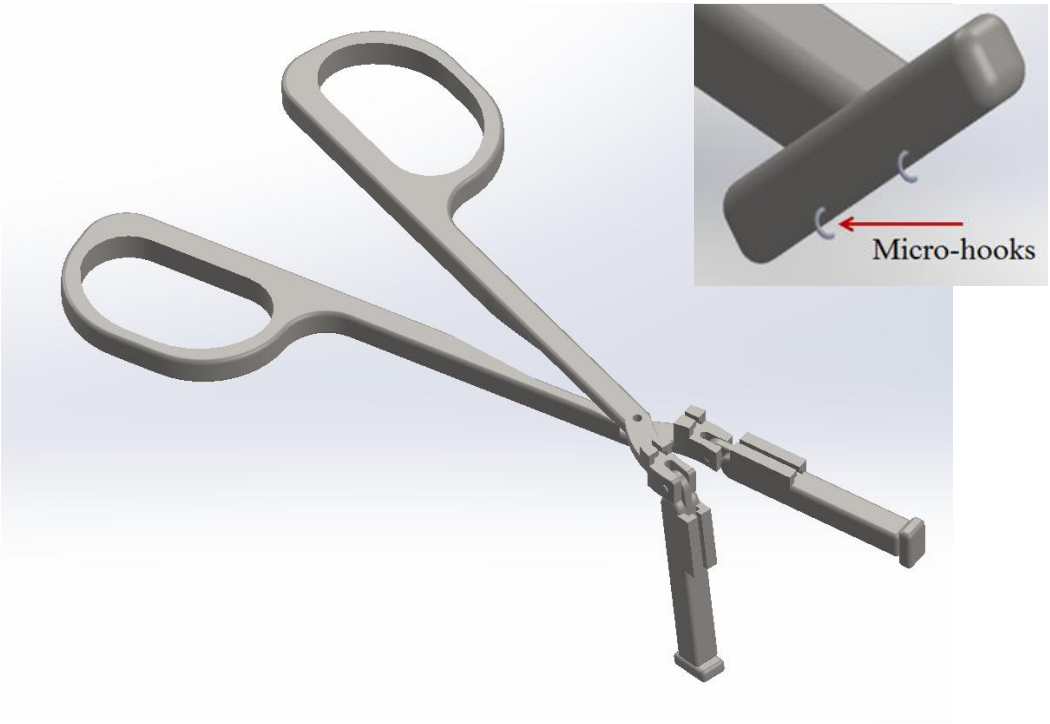

Figure 4.10: Conceptual design locked straight in the far leg and bent in the closer leg. Inset-micro hooks for attachment.

The surgeon would begin by attaching the forceps beds to the deep fascia in the straightened position. The forceps arms would then be pulled together, applying tensile forces to the deep fascia. Once the desired tensile forces have been reached, the ratcheting mechanism (not pictured) could be locked, holding the tissue in place. If the tensile forces are considered to be too significant and a gradual closure is preferred, the surgeon can leave the forceps in place and allow the tissue to creep. Suturing could take place at the discretion of the surgeon. As the incision is sutured, the forceps would be moved up the wound in 1cm increments, displaying strain measurements at each attachment point, and aiding the surgeon in determining the ideal closure process.

4.6 Feasibility Study

A series of studies were conducted to determine the practicality of the design components. First a set of calculations were completed in order to assign the necessary dimensions to the device.

Then the appropriate strain gages and data collection method were chosen to optimize the functionality of the entire device.

4.6.1 Design Calculations

The dimensions of the forceps were then determined through a force analysis to ensure that the device was feasible. The moments on either side of the pivot needed to be equal to allow for rotation about that point. The average forces that the human hand can exert through different types of grips were researched and it was determined that when medical professionals are generally using forceps, a palmer pinch is used. This type of grip, shown below in Figure 4.11, occurs when the thumb pad is pressed against the pads of the index and middle finger (Mathiowetz, 1985).

Figure 4.11: Visual representation of palmer pinch (Mathiowetz, 1985).

The forceps were designed so that any medical professional can use them, and therefore the lowest average force value was used to accommodate all individuals. Table 4.4 below shows the average palmer pinch force values for left and right-handed males and females. As can be seen, the lowest reported value is left-handed females, and therefore a force value for the grip of 69.8N was used during the force analysis to accommodate the weakest grip (Mathiowetz, 1985).

Table 4.4: Palmer pinch strength of left and right-handed males and females (N) (Mathiowetz, 1985).

	Male	Female
Left Hand	102.3	69.8
Right Hand	104.1	72.5

For the force acting on the forceps by the fascia, the pullout strength of the deep fascia was researched. Because the model contains hooks that pierce the deep fascia, it was determined that

the deep fascia would experience failure due to exceeded pullout strength rather than ultimate tensile strength of the tissue as a whole. From this realization, the average pullout strength was found to be 58.2N from a suture pullout study in the deep fascia (Campbell, 1986).

After determining the two forces acting on the forceps, the dimensions could then be calculated from the moments. The dimensions that were calculated are shown below in Figure 19. In order to maintain the dimensions within the standard 8" forceps size, the number of hooks used for attachment was calculated to be two. The overall force acting on the forceps' bed is therefore the pullout strength of the fascia multiplied by the number of hooks, resulting in a force of 116N. The location and direction of the forces acting on the forceps can be seen below in Figure 4.12. The force of the grip is acting at points C and D, while the pullout strength of the fascia is acting at points E and F.

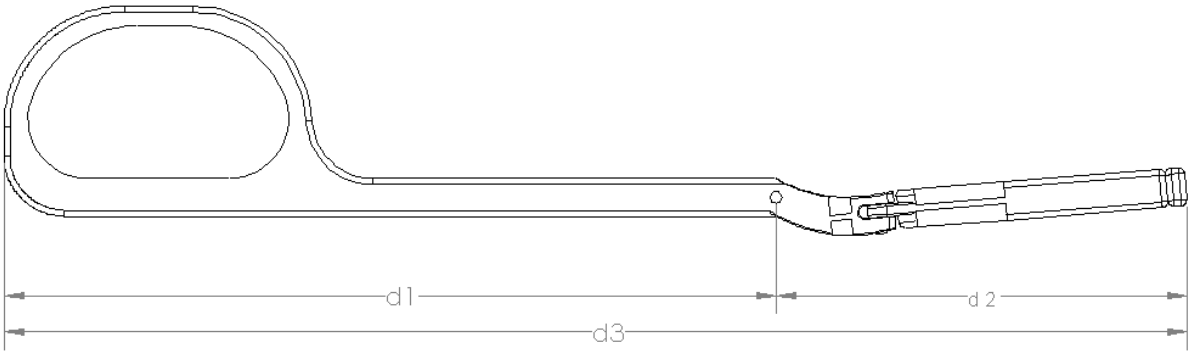

Figure 4.12: Dimensions that were calculated from moment analysis.

The corresponding moment equations were determined incorporating the distances noted above as well as the forces acting on the forceps. These equations are shown below, and from setting the total length of the forceps to be 8", the lengths of d1 and d2 could be calculated. This resulted in a length from the end of the handle to the pivot to be approximately 12.7cm, while the length from the end of the forceps' bed to the pivot was approximately 7.6cm. These calculations were then used to create the computer aided design model in SolidWorks, ensuring that the moments would balance out and the forceps could rotate about the pivot point while applying enough force to close the deep fascia with the weakest grip.

$$d2 := \frac{Fg \cdot d3}{Ff + Fg} = 7.6\,cm$$

$$d1 := d3 - d2 = 12.7\,cm$$

4.6.2 Strain Gage Selection and Data Collection

The next step in finalizing the design was to determine what strain gage (seen in Figure 4.13) would be necessary as well as where the ideal location would be along the length of the forceps. There are several aspects that are a part of strain gage selection that vary depending on the type of strain gage. These different characteristics include a strain-sensitive alloy, backing material or carrier of the gage, grid resistance, gage pattern, self-temperature compensation number corresponding to temperature-induced strain, gage length, and other options that are available. It is important to select the strain gage based on how it will be applied and the environment in which it would be used, but also taking into consideration constraints such as accuracy, temperature, and cyclic endurance (Vishay, TN-505-4). More information on the selected strain gage can be seen in Appendix M.

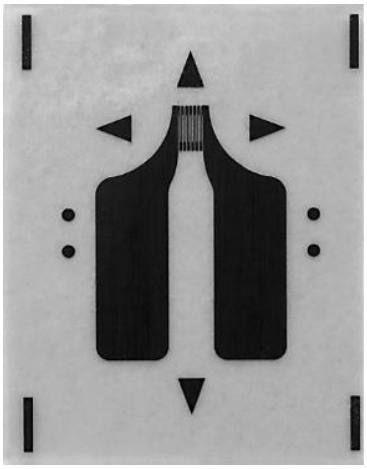

Figure 4.13: Strain gage selected to be used on final design (Vishay, TN-505-4).

It was then necessary to determine the location on the forceps to place the strain gage. It was decided to have a strain gage on each side of one arm to obtain measurements in both tension and compression to compensate for temperature effects that may occur. The location on the arm was a significant part of the design to obtain the maximum amount of strain in the material. Through the creation of a moment diagram, the maximum strain experienced was determined to be at the

pivot. Therefore, it was decided that the strain gage needed to be located as close to the pivot as possible on the outsides of the arms.

Data collection was initially conducted through the most basic means. The strain gage is wired to an amplifier, which increases the micro strain measurements by ten, and ultimately transmitted to a Digital Voltmeter. On this screen was where the volts were displayed in millivolts. The full setup of the equipment can be seen in Figure 4.14 below.

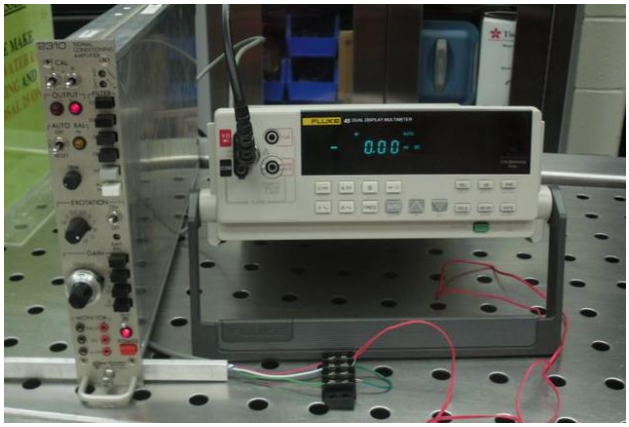

Figure 4.14: Setup of equipment used for data collection. Left is the amplifier; right is the digital voltmeter

4.7 Preliminary Data

The following tests and preliminary data sets were conducted to analyze the functionality of our design. Initially, the factor of safety of the hook attachment was determined. Analytical calculations were completed to ensure that a strain gage would be capable of reading the small amount of deflection in the material. Lastly, mechanical testing was conducted on the material to determine the radius of curvature experienced.

4.7.1 Factor of Safety

The factor of safety was calculated in order to confirm that the two micro-hook design would not cause excessive damage to the patient when the device was applied to the deep fascia of the abdominal wall. In order to perform these calculations, which can be seen below, a value of 10lbf was hypothesized to be the average maximum applied force to the deep fascia. This value is close to the force of the deep fascia during suture pull-out testing which was found to be 60N, but does not exceed it. The force per hook was calculated by dividing the applied force by the number of hooks, 2. Dividing the force of the deep fascia during suture pull-out testing by the

force per hook and multiplying by 100 results in a percentage correlating to the factor of safety. The calculated factor of safety at two hooks under a load of 44.5N was 270%, which indicates that the tissue will be safe from potential tearing during the application of the device. These initial calculations allow for the conclusion to be drawn that the two micro-hook design would offer a substantial buffer against potential damage to the deep fascia outside of the average applied maximum force value of 44.5N.

$Ffascia := 60N$ Force of the fascia

$Fapplied := 10lbf = 44.5\,N$ Force applied

$Nhooks := 2$ Number of hooks

$Fhook := \frac{Fapplied}{Nhooks} = 22.2\,N$ Force per hook

$SF := 100\frac{Ffascia}{Fhook} = 269.8$ Safety Factor (%)

4.7.2 Analytical Strain Calculations

To confirm that the hemostats would be subjected to a high enough load to cause a deflection and therefore a strain large enough to be read by the strain gage, analytical calculations were performed. The hemostats were analytically loaded according to the force of the grip (70N). Using the distance (d) from the handle to the location to the strain gage, which was estimated to be approximately 0.13m, the moment (M) about the handle was calculated. The moment was determined to be 9.1J.

$Fgrip := 70N$

$d := 0.13m$

$M := Fgrip \cdot d = 9.1\,J$

The moment of inertia of the handle was calculated according to the dimensions of the handles. The hemostats are square in shape, having a height and width of 0.00635m. Calculations for the

moment of inertia (I) can be seen below. The moment of inertia was calculated to be 1.4×10^{-10} m^4.

$$h := .00635m$$

$$I := \frac{1}{12}\left(h^4\right) = 1.4 \times 10^{-10}\, m^4$$

Using the values calculated for moment and moment of inertia, the expected stress could be calculated, as seen below. The distance to the centroid is equivalent to one half the height (h/2). With the value for Young's Modulus for stainless steel taken as 200GPa (E) and Hook's Law, the expected strain could also be calculated.

$$Fgrip := 70N$$

$$Stress := \frac{\left(M \cdot \frac{h}{2}\right)}{I} = 2.1 \times 10^{8}\, Pa$$

$$E = 200\, GPa$$

$$Strain := \frac{Stress}{E} = 1.1 \times 10^{-3}$$

The expected strain value of 1.1 x10-3 indicates that the hemostats when loaded with a force of 70N will experience a strain large enough to be detected by the strain gages. The force of the grip value of 70N is considered the minimum amount of force that the hemostats would be loaded with. Keeping this in mind, it can be stated that as force of the grip increases, the hemostats will experience larger strains.

Chapter 5: Design Verification

This chapter presents the data that was obtained to verify the final design. A series of prototypes were created to ensure ease of use and validate the design. Data included was collected from finite element analysis (FEA) of the initial and final prototype, swine testing, and refining the circuit, which has previously been outlined in Chapter 3. The success or failure of these preliminary data was used to modify the current design to satisfy all aspects of the project goal.

5.1 Finite Element Analysis Validation

Validation of the FEA software was completed by conducting the analysis on a constant volume stainless steel bar in order to compare these values with analytically calculated strains. The percentage error between the two models was then determined to ensure that the finite element model was within 9% of the actual value.

5.1.1 Analytical Model

Four different force magnitudes, 2.5lbf, 5lbf, 7.5lbf, and 10lbf, were used to develop the complete data set. These values were based off of the weights that were available to be used for the calibration of the strain gage later on in the verification. The distance from the handle to the center of the strain gage was used for the analytical calculations, which was measured to be 97.5mm. This was determined from assuming the approximate distance of the edge of the strain gage to the pivot to be 2mm, while the length of the strain gage was 6mm. The dimensions of the hemostats were based off of the initial prototype specifications during this FEA verification testing period, in order to ultimately calibrate the strain gage using these results. The height and base of the handles were considered to be 6.35mm. The moment of inertia was then calculated as previously described.

From there, the moment was calculated to determine the amount of stresses that occur at each force magnitude.

$$M := F \cdot d$$

These moments then corresponded to the stress equations.

$$\sigma := \frac{M \cdot h}{2 \cdot I}$$

Using these stress values and the Young's Modulus of stainless steel 316L, the theoretical strains that the material would experience were able to be calculated.

$$E := 200GPa$$

$$\varepsilon_g := \frac{\sigma}{E}$$

The calculated results can be seen below in Table 5.1.

Table 5.1: Theoretical calculations for the moments, stresses, and consequent strains the material will experience at four different force magnitudes.

Force (lbf)	Moment (N-m)	Stress (Mpa)	Strain (m/m)
2.5	1.1	25.4	1.3E-04
5	2.2	50.8	2.5E-04
7.5	3.3	76.2	3.8E-04
10	4.3	101.6	5.1E-04

5.1.2 FEA Model

The constant volume stainless steel bar model was then imported into ANSYS from SolidWorks, and a mesh was created to divide the model into its elements. Constraints consisting of a fixed support at the far end of the beam at point A and the load on the near end at point B were then placed on the model.

For the resulting data sets that we were interested in, we began by examining the normal stresses along both the X and Y axes. The results of these data sets confirmed, as you can see below in Figure 5.1, that the material experiences essentially zero stress in the Y direction, also confirming that no strains would be experienced in this direction as well. A line segment was

created on the model indicating the position of a strain gage, with the location that was noted previously: 2mm from the pivot with a length of 6mm. Because the material experienced no stress in the Y direction, it was determined acceptable to simplify the analysis and make a straight line for a path along the X direction rather than focusing on the entire surface area.

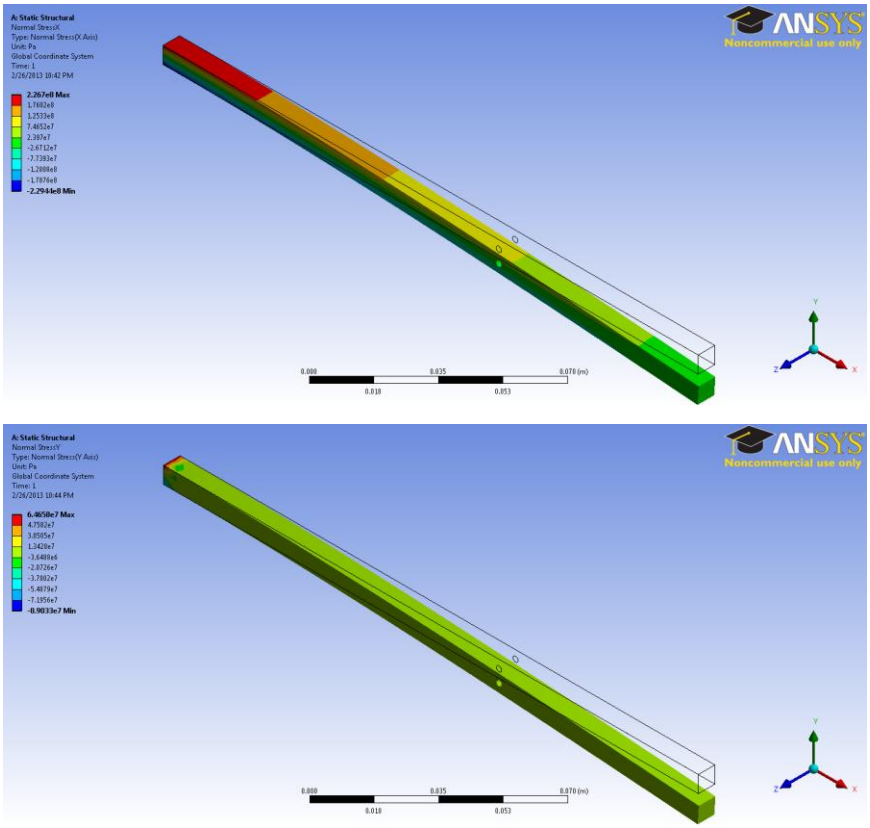

Figure 5.1: Top-FEA results for the varying stresses along the X-axis Bottom-stress along the Y-axis, essentially zero in the Y direction

The normal strains and stresses were then calculated along the path to be directly compared to the theoretical values calculated previously. The results along the strain gage were exported to an excel file and the average of the data was taken. This represents the process of data acquisition of a strain gage, as the average along the length of the gage in each direction is taken. The results of the strain analysis can be seen below in Figure 5.2, while the graph displaying the slight variation in strains along the length of the strain gage can be seen in Figure 5.3. This graph represents a realistic reading of strain measurements that would be experienced along the entire length of the strain gage, and the average would be the output.

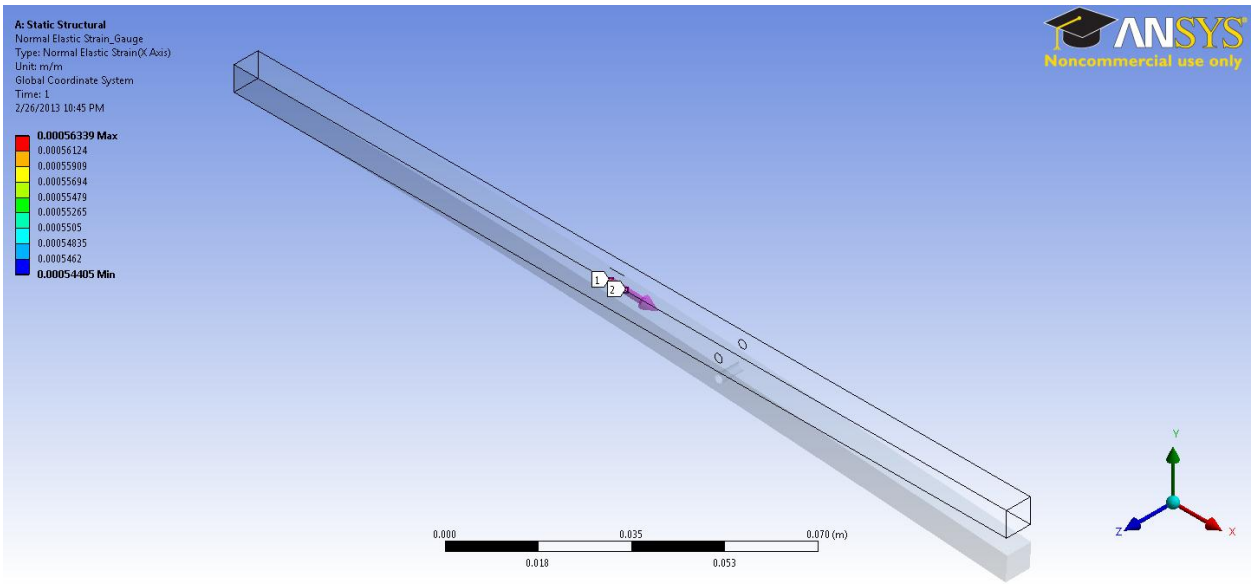

Figure 5.2: FEA normal strain results in the X direction along the strain gage path.

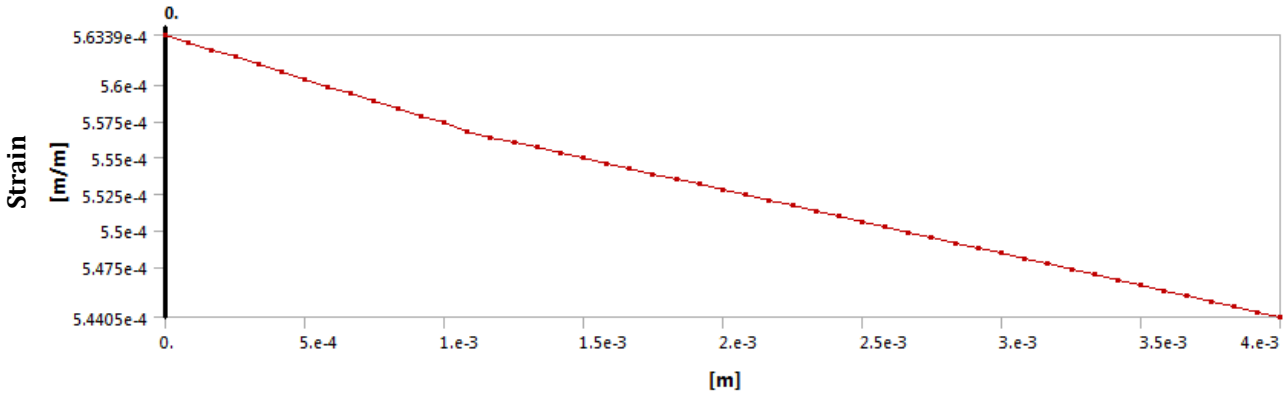

Figure 5.3: Graph exported directly from the FEA results showing the slight variation in strain along the length of the strain gage.

This process was repeated with the four magnitudes of force as the analytical calculations. The two different analyses were then compared. The results can be seen below in Table 5.2.

Table 5.2: Comparison of the results between the analytical calculations and the FEA results for the strains along the X axis.

Force (lbf)	Strain (m/m) Analytical	Strain (m/m) FEA
2.50	1.3E-04	1.4E-04
5.00	2.5E-04	2.8E-04
7.50	3.8E-04	4.2E-04
10.00	5.1E-04	5.6E-04

The results of the strain calculations show that with the two sets of comparisons resulting in a small percentage error between the two, it is able to be concluded that the FEA results are reliable means of analyses.

5.2 Rapid Prototype

The first prototype was created using the rapid prototype machine in which the model was replicated by a plastic model, seen in Figure 5.4. The purpose of this prototype was to determine the ease of use of the hinge by evaluating the mechanism for which the hinge could be locked as well as the pivot point of the hemostats. Through the use of CAD software, aligning each arm to be locked straight was a challenge. When the prototype was created by the rapid prototype, the hinge was confirmed to be useful in minimizing interference with suturing; however a few stages of redesigning were necessary to refine the locking hinge. This helped with ease of use and manufacturability.

Figure 5.4: Image of the rapid prototype showing the hinge mechanism

Additionally, the first pivot design was discovered to cause the hemostat legs to be unequal lengths. This would not be useable for the design since the attachment to the fascia would not be the same for each side. When the hemostat arms are locked in the straight position, the arms would not be on the same plane due to the difference in the thickness of each arm. Therefore, it was recognized that the final design would need the pivot design that is implemented for the common hemostat to operate correctly.

5.3 Initial Prototype

The initial prototype that would be used during animal testing was developed from a 12-inch pair of stainless steel hemostats is shown in Figure 5.5 below. The lengths of each segment were measured based on the calculated proportions from Chapter 4. The thickness of each arm however was larger than designed, but would serve the purpose for this initial prototype. The locking hinge was omitted in this prototype due to the difficulty in machining the device with resources that were available. The focus was to test proof of concept concerning the strain gage, ease of use, and other necessary design modifications.

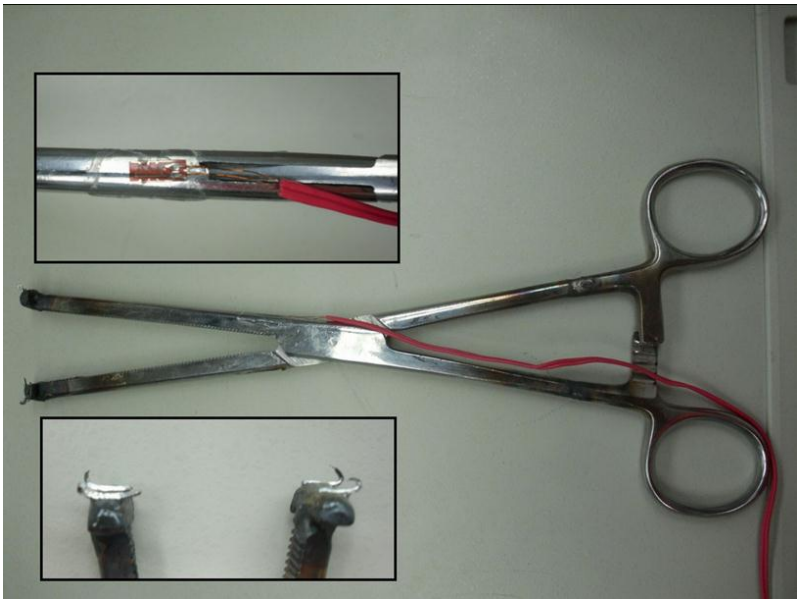

Figure 5.5: Initial Prototype Top Inset-strain gage, Bottom Inset-microhooks made from suture hooks.

5.3.1 Calibration

Prior to using the initial prototype for animal testing, the strain gage needed to be calibrated. This was done by fixing the handle end of the hemostats and applying a known force to the attachment location, and recording the resulting strain readout. Using the four different weights discussed previously in the FEA validation, a relationship between the forces applied and the strain reading was determined and a calibration factor was developed. Using the calibration factor calculated previously, it was found that approximately 90mV was equal to 9lbf.

5.3.2 Swine Testing

Swine testing, discussed in Chapter 6, was conducted partially for proof of concept and design amendments. Specifically discovered through this testing was the attachment angle. It was discovered that the 45 degree angle would offer the most comfortable position for the surgeons to apply the tensile forces. The attachment mechanism was adjusted to better achieve the atraumatic attachment and detachment efficiently. Replacing the two original micro hooks was a rake, which has been designed by KLS Martin to operate as a skin retractor. This increased number of hooks on the rake, from two to five, led to a stronger attachment point with minimal slippage. A greater number of hooks that would penetrate the deep fascia would increase the factor of safety and thus decrease the risk of causing further complications.

5.4 Final Prototype

The final prototype was produced to mimic the final design as close as possible. Unfortunately, the machining capabilities that were available at WPI led to design changes. This prototype contained a hinge, and pivoting rakes attached to the legs of each hemostat arm.

5.4.1 Calibration

Similarly to the initial prototype, the strain gage on the final prototype also needed to be calibrated. This was done using the same methods described previously: fixing the handle end of the hemostats and applying a known force to the attachment location, and recording the resulting strain readout. Using the four different weights discussed previously in the FEA validation, a relationship between the forces applied and the strain reading was determined and a calibration factor was developed.

5.4.2 Design Modifications

The aspect of the device that this most affected compared to the final design was the attachment of the rakes. Since the rakes ordered from KLS Martin are on a tapered handle, they were unable to be press fit. This created the task of designing a new method by which the rakes could be attached. Another challenge to overcome was that the stainless steel of the rake was hardened to increase mechanical strength. Unfortunately, this increased the difficulty of machining these parts. Kept in mind was the ability to pivot the rakes and also the minimally sized gap that would be formed when the device is completely closed.

After a few design iterations, the final prototype was created using a bolt and nut design. A hole drilled into the side of the nut created a space for the rake to be slid into, as can be seen below in Figure 5.6. When the bolt was slipped through the leg, the bolt would be tightened which in turns locks the rake into place. This design allows the rake to pivot within the nut during use of the device. The final prototype, seen in Figure 5.7, was completed for further testing and evaluation.

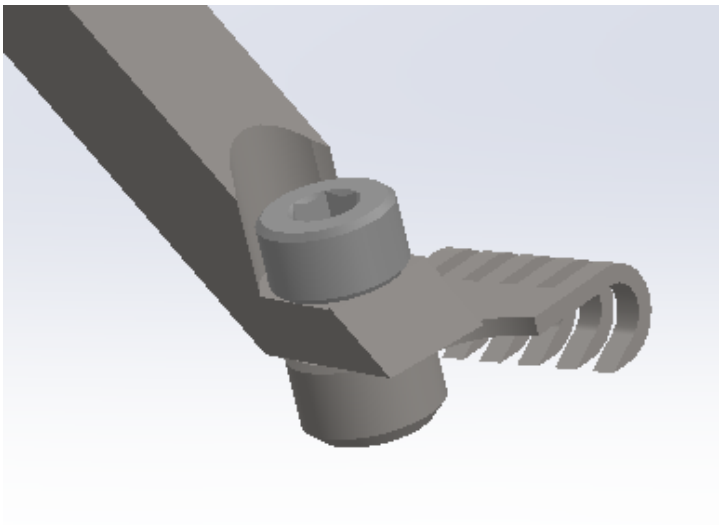

Figure 5.6: Machine modifications showing the rake attachment method.

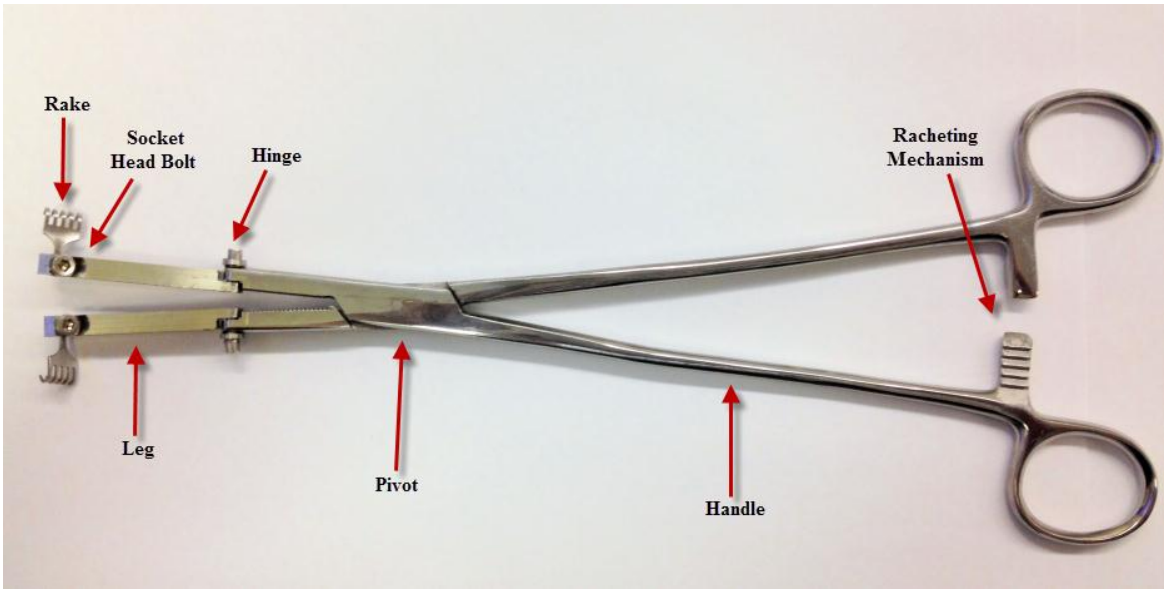

Figure 5.7: Machined final prototype shown in straightened position. Note that the locking collars are not present.

Chapter 6: Results & Discussion

Initial testing was conducted on swine cadavers at the UMMS necropsy lab that lead to initial data collection and design modification. Through this testing the functionality of the device was able to be further refined. A major factor influencing data collected was the time of death of the swine, which was responsible for increasing the stiffness in the abdominal tissue. Prior to testing and data collection, swine had been euthanized: the first swine was euthanized at approximately 5 hours prior to testing, and the second swine was euthanized more than 24 hours prior to testing. After euthanization, swine were preserved in the necropsy morgue.

6.1 Fish Scale Weight Testing

Fish scale weights were used to gage the force applied to the deep fascia during closure of the incision. The forces measured showed some variance, but it is important to note that sample size was very limited, and there was not enough data to conduct an accurate statistical analysis. The average forces applied to the deep fascia to close the incision are shown in Table 6.1.

Table 6.1: Force measured in the abdominal wall of the swine using fish scale weights

Swine (weight)	Left Side	Right Side
Trial 1 (35 kg)	4 pounds	4 pounds
Trial 2 (27 kg)	5.37 pounds	5.5 pounds

6.2 Swine Trial Testing

Anatomical differences of the abdomen between human and swine are too significant in order to develop an accurate numerical relationship, however the methods for data collection and analysis would remain the same. Therefore, swine testing was used solely to verify the protocol for application of the device as well as to develop methods of analysis that can be used for interpreting human data.

The first trial of swine testing presented some difficulty in gathering useful data. From the multiple attempts of attachment and closure, only three trials produced meaningful data. Figure 6.1 below shows the plots of each trial representing the voltage versus time. Each set of data was

different due to the imperfect application of the device. This ultimately resulted in a skewed data set; however methods for converting voltages to strain were confirmed using the data regardless.

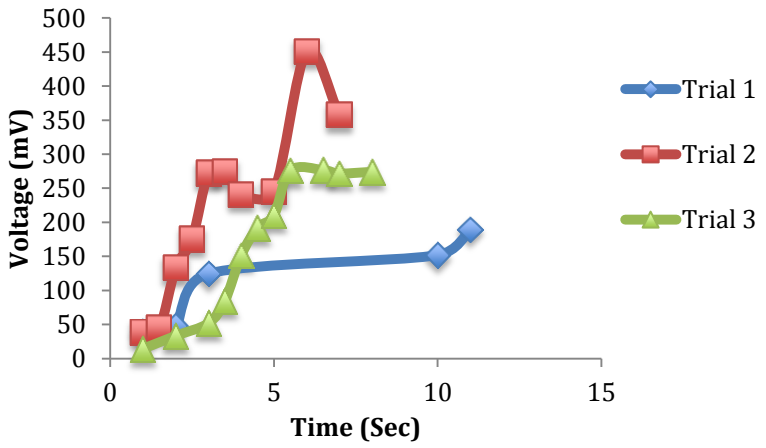

Figure 6.1: Plot of voltage versus time for the first set of swine data.

Trial 1, with a maximum of 189.3mV, was much lower than the other two trials because of slippage at the attachment point, causing the hemostats to disengage from the deep fascia. The trial that demonstrated the best use of the device was trial 2, where the abdominal tissue was pulled to proper positioning for suturing. The highest voltage was recorded at this point to be 450mV that at first glance, seemed substantially larger than the value that was anticipated. The volts were then converted into stress, shown below, using the calibration factor previously determined through weight testing, 10mV corresponds to 1lbf and therefore the maximum voltage can be converted to approximately 5lbf. This is consistent with the fish scale weights previously discussed.

Attempts at analyzing the plot for trial 2 presented no useful data. A trendline was fit to the curve of trial 2, but due to the inconsistent data collected over a time period, and small sample size, the curve was determined not to be reliable. Different parameters for the analysis need to be used in order to produce useful data. The most important value under investigation is the maximum voltage at the point of closure, which can be correlated to the applied force. However, in order to develop a pattern or prove a statistical similarity, relating the voltage measurement to the incision width would be most beneficial. This would allow a relationship to be formed between voltage and width of wound for multiple patients.

6.3 Design Modifications

Swine testing using the initial prototype revealed that certain aspects of the device required modification, specifically the details concerning the attachment method. The size and shape of the two micro-hooks and angle of attachment were reevaluated. The suture hooks that were modified to represent the final design were roughly bent into the curved shape with the smallest diameter that could be achieved, but there was a lack of uniformity amongst all of the hooks. The size and curve of the hooks clearly effected the attachment: hooks on the left arm of the hemostat were not as curved as the right side and thus did not have the same success rate in which the hemostats were engaged in the tissue. Also, the sizes of the hooks were just slightly too small to grip enough tissue and therefore, the size needed to be adjusted.

From the swine testing previously conducted, it was estimated that the applied force would range from 4.5lbf-10lbf. Analysis of previous data showed the maximum result to be 9.17lbf. For this reason, the safety factor per number of hooks was calculated at each of these values in order to determine the optimal number of hooks to be used in the design. It was important to consider the time of death of the pig, which ranged between 24 and 48 hours because it has a stiffening effect on the abdominal tissue. The results are shown below in Table 6.2.

Table 6.2: Safety factor percentages based on measured forces of swine fascia

Number of Hooks	4.5 lbf	9.17 lbf	10 lbf
2	600%	294%	267%
4	1200%	589%	533%
5	1500%	736%	667%

Comparing the factor of safety from the swine data and the hypothesized range, it was found that the 5 hook design is the best option. This accounts for a high enough buffer to prevent excessive force that could have the potential to tear the deep fascia. Further discussion with the client confirmed his preference for a rake design consisting of multiple micro-hooks.

It was also observed that the angle of the beds of the rough prototype would require a surgeon to approach the wound at an uncomfortable angle, nearly perpendicular to the tissue. To account for this, the beds were angled to approximately forty-five degrees, which would allow for a natural

angle at which the device could be used. This angle was suggested by Dr. Raymond Dunn. This modification was the amended for the second final prototype.

6.4 Human Testing

Feasibility testing with the final prototype was conducted in the operating room under the guidance of Dr. Raymond Dunn, as seen in Figure 6.2 below. The hemostats were applied to the deep fascia and used to pull the edges of the incision closed. The general function of the device was successful. However, the machining modifications of the final prototype elicited a few fine adjustments to note for the final manufactured design. First off, the modification for rake attachment allowed too much left to right motion and caused difficulty with proper attachment. This imperfection was considered for final manufactured device. During attachment and closure of the incision, the legs of the hemostats did not remain in straightened position, which confirmed locking collar as an essential component of the device design. Overall, human testing demonstrated that the hemostats are capable of attaching to and detaching from the deep fascia atraumatically and can apply localized tensile forces at the site of attachment.

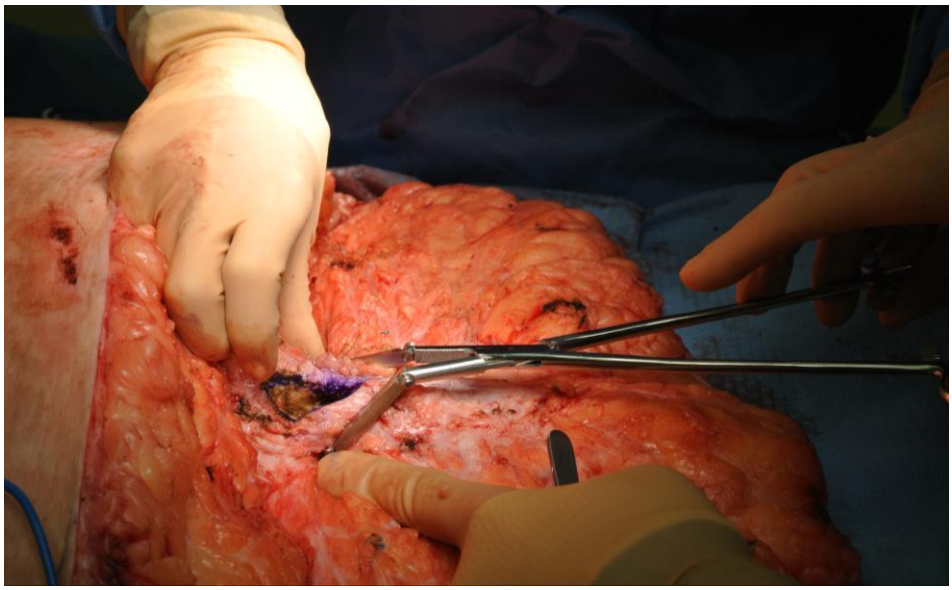

Figure 6.2: Final Prototype Testing in the operating room during incision closure

Chapter 7: Final Design and Validation

The final device description is presented in the following chapter outline the detailed components, their functions, and the recommended use of the device. Additionally, FEA of the CAD model was evaluated to validate the final design. Data collection methods are also discussed, specifically the circuit constructed to work in unison with the hemostats.

7.1 Final Device Design

After producing a rapid prototype and an initial prototype, the design of the hemostats was finalized to the model seen in Figure 7.1. The final design consists of a pair of specialized hemostats with hinged arms, rakes for attachment, and two strain gages. The overall length of the hemostats is 21cm, keeping it similar to the standard 20cm hemostat range. From the hinge to the hemostat bed is 5cm to accommodate wound thickness. The thickness and width of the hemostats' arms are 4mm.

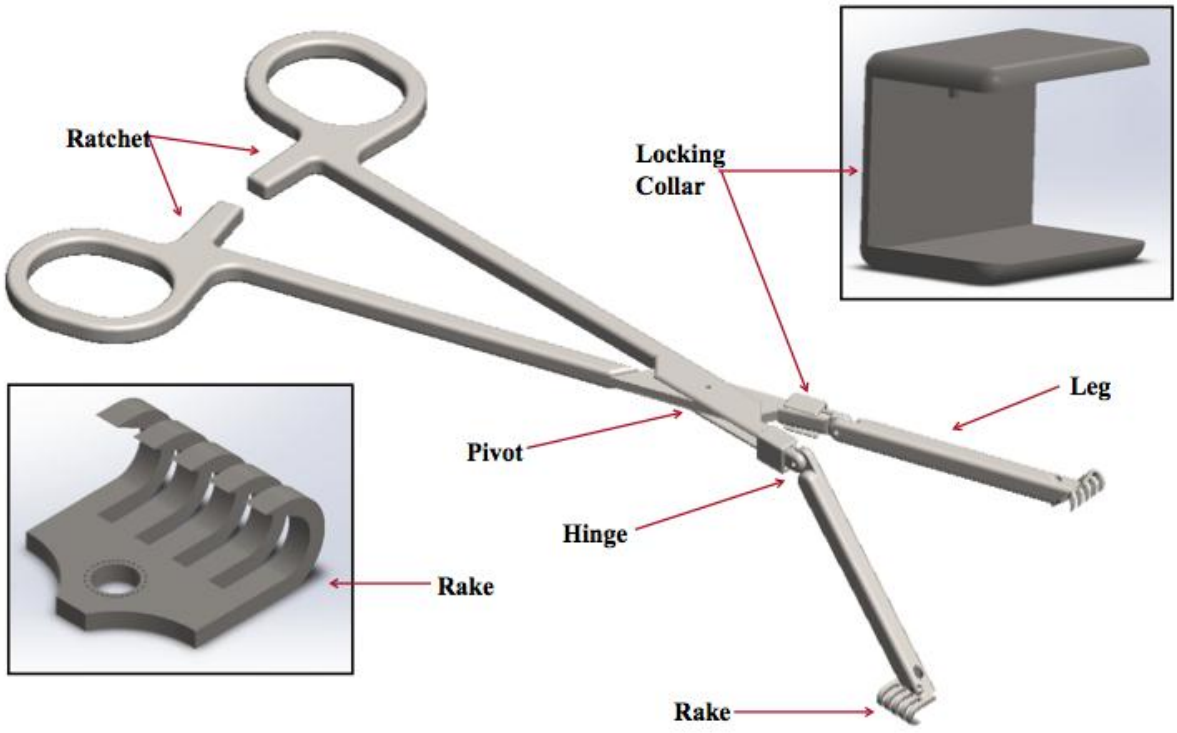

Figure 7.1: CAD Model of Hemostats. Upper right insert shows a close-up of the locking collar. Bottom left insert shows a close-up of the rake used for attachment. Visible are both straightened and bent positions.

It was designed to be applied to the deep fascia during approximate closure of the wound without puncturing the peritoneum and to not be an obstacle for surgeons. A rake was selected as the optimal attachment method because it offered a high factor of safety (674%) while securing well to the deep fascia, which has been reported to be 156μm on average (Stecco, 2011). To ensure that the rakes would consistently attach parallel to the deep fascia, they were equipped with a pivot to allow left to right motion. Two key elements of the design were the 45° angle of the rakes which allow the surgeon to approach the incision comfortably and the hinge, which enables the surgeon to bend the handles of the hemostats out of the way while suturing. The hemostats have two major positions: straightened position, when the hinge cannot articulate because the locking collar is in place, keeping the hemostat arms completely straight; and bent position, when the hinge can function and the handles can be bent backwards.

Located on the interior and exterior sides of one hemostat arm in the direction of the handle are two Vishay TN-505-4 strain gages, which consist of a linear micro-miniature pattern and are able withstand temperatures ranging from -320°F to +350°F (Vishay, 2012). The strain gages were bonded as close to the pivot as possible, where the maximum moment occurs, a location which was confirmed by Finite Element Analysis. Additional epoxies were used to protect the gage from moisture during autoclaving. Silver plated copper lead wiring was used to ensure that the entire device would be autoclavable (Vishay, 2012).

The lead wiring was then connected to the circuit that would be responsible for amplifying the micro strains displaying the voltage on a handheld voltmeter. The circuit would be located outside the sterile field within the operating room. The two strain gages would be connected in series in a full Wheatstone bridge which can be seen in the schematic show in Figure 7.2. Balancing the full bridge, two 200Ω resistors, and two potentiometers were added. Two potentiometers were used in order to calibrate the resulting voltages and zero the scale. The first part, 102 was used for coarse adjustments while the second, 101 was used as fine adjustments. This full bridge was then connected to the non-inverting amplifier, LM324N with the input traveling through the positive. The 200kΩ resistor and the 100Ω resistor were chosen to accomplish the 1V fluctuation that could be read through the circuit. The positive and negative outputs were attached to the corresponding wires of the hand held voltmeter. The channel for the

voltmeter was changed based on the battery that was used. Testing of the circuit used a 5V input however the final circuit will use a 9V battery.

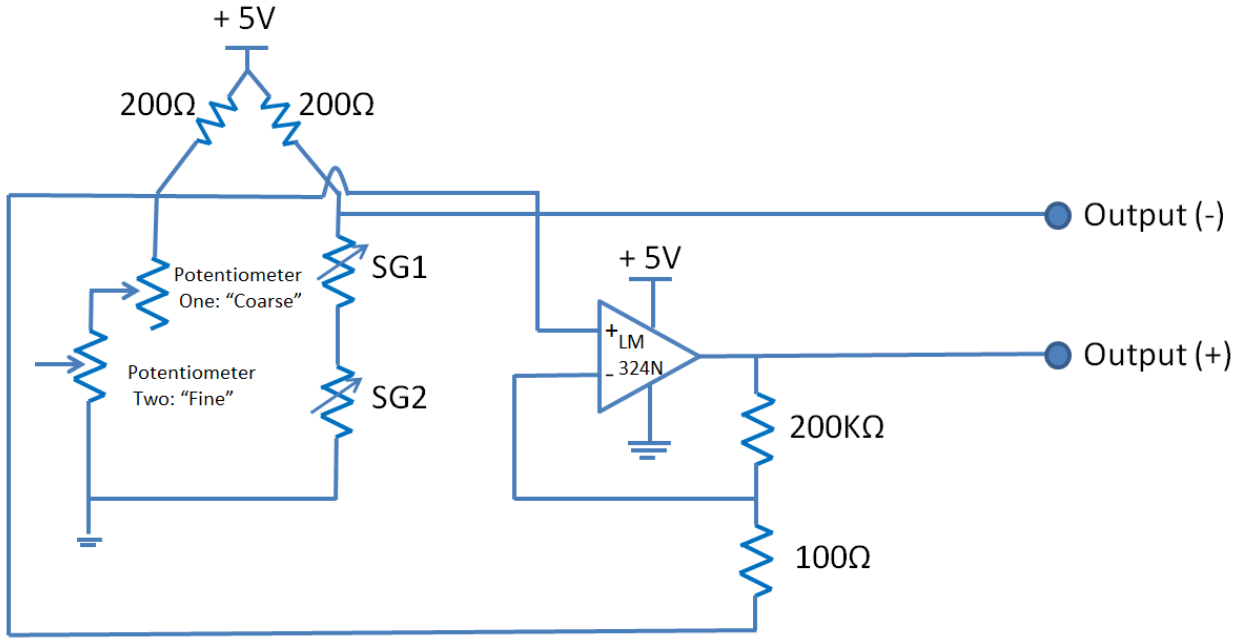

Figure 7.2: Schematic of the full Wheatstone Bridge and amplifying strategy.

7.2 Finite Element Analysis Model

FEA was conducted on the final model most importantly to ensure that the design would not fail under maximum loading. To analyze this, one arm of the CAD model was assembled and imported to Ansys to be evaluated. The forces and point of fixation were applied to mimic the application of the hemostats during closure. Therefore, the pivot point was fixed in place, indicating where the moment is zero and there are no acting forces. The force applied by the surgeons hand was located on the handle of the hemostat in negative x-axis and the force applied to the deep fascia was also applied in the negative x-axis at each point of the rake.

The force value that was applied to the handle was 70N based on the force of the grip, mentioned in Chapter 5. Also discussed previously was the suture pull out strength measured in the deep fascia, which attributed to the maximum force that could be applied to the deep fascia at an individual contact point. This was the rationale for applying 60N of force at each of the five points on the rake.

The following stresses were examined to confirm that the integrity of the device would remain sound. Along the length of the arm, it can be seen in Figure 34 that the stresses were all dark blue indicating a minimum of $1.1x10^{-5}$ MPa. It was discovered that the highest areas of stress were located at along the sides of the hinge as well as the circumference of the pin holes. Figure 7.3 below shows the locations at which the experienced stresses are higher. The stresses at these points vary between 1500 and 6300 MPa. The maximum stresses that were seen are not proper representations of how the device would respond to the forces applied due to imperfections in the CAD model. Most importantly, these stresses are targeted along the edges at which the features contain sharp edges, not realistic for machining. Similarly, the corners experience unnaturally high stresses as well do the identical modeling discrepancy. Reporting these values as unrealistic outliers in the data, the stresses experienced along the entirety of the hemostat arm are congruent with the ability of the device to remain intact during the maximum possible loading.

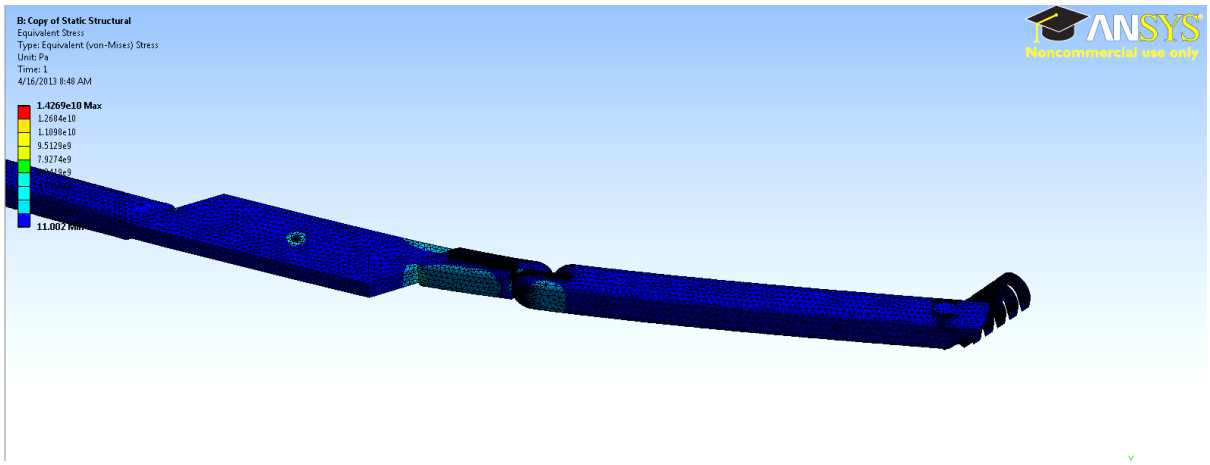

Figure 7.3: Areas of high concentration of stress experienced along the hinge of the device

Further interpretation of the results revealed that the mesh was not best suited and was adjusted for more accurate data. These points of high stresses can therefore be analyzed as outlying factors that do not properly represent the true stresses that would be experienced. The change in the mesh can be seen in Figure 7.4 below. Additionally, the original mesh that was assigned did not properly encompass the geometry of the device. The second mesh had a higher number of elements and therefore better represented the model however some sections were over defined, such as in the handle. The second mesh was more accurately representative of the stresses in the hinge.

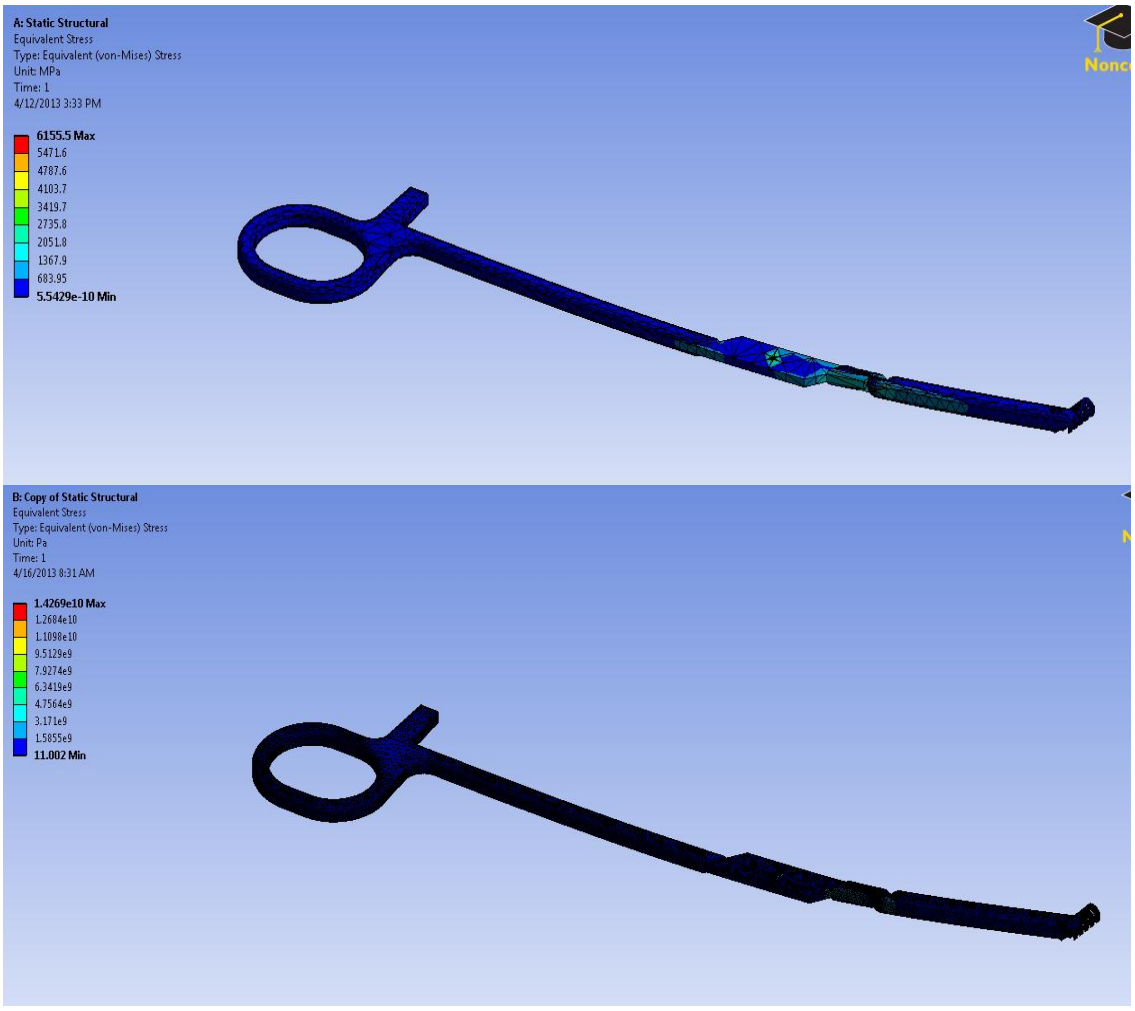

Figure 7.4: Top-original mesh with poor geometry, Bottom-Modified mesh with a greater number of elements.

7.3 Methods for use of Final Design

Before the hemostats are applied in surgery, they must autoclaved to preserve patient safety and sterility of the operating room. The hemostats are constructed from medical grade stainless steel 316L, and are capable of withstanding the heat and moisture of the autoclave. The strain gages bonded to the hemostats are coated in a specialty epoxy and rubber to lock out moisture. Silver plated copper lead wiring connected to the strain gage is also autoclavable. The circuit containing the signal conditioning chip and handheld voltmeter will remain outside of the sterile field.

After the completion of a midline laparotomy, the surgeon will begin to the close the incision. This process begins by bringing the edges of the wound to approximate closure, where the tissue is separated by a minimal distance. Then, the hemostats, in straightened position, are attached to

the deep fascia using the rakes, and used to pull close the tissue. While the hemostats are in straightened position and tensile forces are being applied, strain measurements are recorded through the use of a strain gage conditioning chip and a handheld voltmeter. When ready for suturing, the ratcheting mechanism can be used to lock the hemostats in place, and the locking collar is slid backward releasing the hinge and allowing the hemostat handles to bend backwards. After this portion of the incision is sutured shut, the hemostats can be attached to the deep fascia at another location along the incision until it is entirely closed. When the closure process is complete, the hemostats can be autoclaved to maintain sterility.

Chapter 8: Future Recommendations

Although the device created is fully functional and is able to be used in the operating room to conduct clinical trials, the limited budget and time constraints of this project provided some inevitable setbacks throughout the development. Therefore, suggestions for future work on this device are discussed in this chapter. These suggestions include conducting human testing upon IRB approval, developing a wireless circuit, and incorporating a purely mechanical device during closure once the safe levels of tensile forces to be applied are known.

8.1 Human Testing

The successful development of a relationship between levels of tensile forces and safety of closure will require clinical studies involving a wide range of patients. It is hypothesized that the levels of forces will vary based on age, sex, and BMI, and therefore it is critical to incorporate this wide variation in the studies. An IRB was submitted and if accepted, a clinical study can be initiated and data collecting can begin.

8.2 Wireless Circuit

While the wireless circuit is an essential step in moving forward with the hemostats and their application, it is currently in the beta-phase, where it consists of its essential parts, but needs to be further developed and refined. A systematic circuit diagram of the wireless circuit can be seen in Figure 8.1. Specific criteria for the circuit must be considered, with a focus placed on the battery-operated power source and ensuring that the circuit is sterilizable. To achieve the optimum design, is it important to know the extent of battery life, time lapse between charges, and methods of charging or replacement. In order to be used in the operating room, the hemostats and the circuit must be sterile. This requires that the circuit be protected from heat and moisture, and rubber coatings such as silicone should be considered and evaluated for efficacy.

The circuit must then be scaled down while still meeting the design requirements, with the final goal being a completed and fully operational circuit incorporated onto the body of the hemostats. The final circuit would be printed and then recessed into the body of the hemostats, minimizing interference or the possibility of becoming an obstacle to the surgeon. To ensure that the circuit would be autoclavable, it could be coated in PDMS silicone rubber to lock out moisture and heat. More information on this wireless circuit can be found in Appendix N.

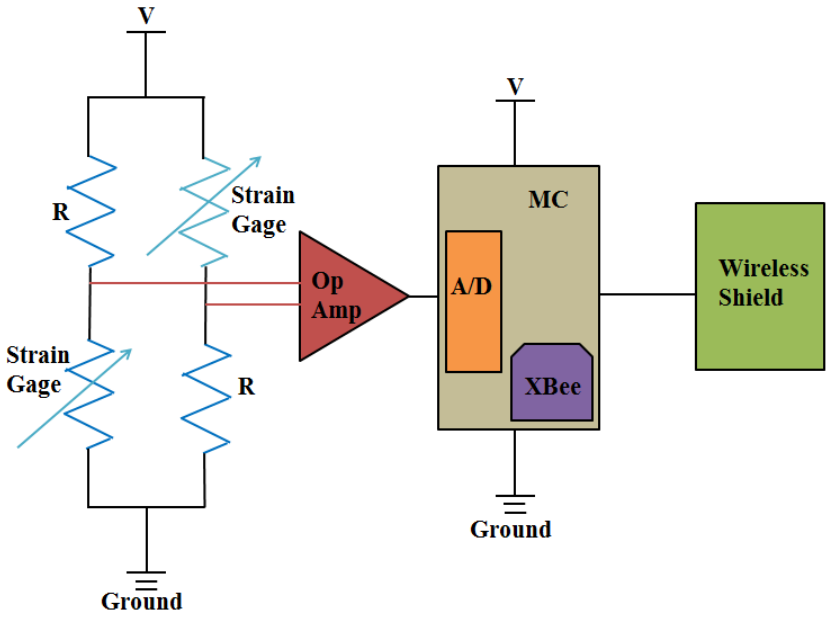

Figure 8.1: Systematic circuit diagram of wireless circuit.

8.3 Purely Mechanical Device

A strain gage was determined as the optimal method for data collection to establish a safe level of tensile forces to be applied to the deep fascia. The strain gage and circuit design allowed for a consistent measurement of the tensile forces being applied which would be compiled and analyzed. Once the full scale clinical study is completed, it is recommended that the purely mechanical variation of the device design be used to eliminate the electrical components and simplify the use of the instrument for future surgical use.

The mechanical design consists of the same basic features that were described in Chapter 7. The instrumented hemostats include: the pivoting rakes for attachment to the deep fascia, the hinge to bend the handles of the device to avoid interference with suturing, locking collar to keep the hinges straightened during application of forces, and ratcheting mechanism found in standard hemostat designs for securing the device at the desired position. The substituted mechanical design is a force indicator that is integrated into one of the handles. The values along the inscribed ruler correspond with the aforementioned relationship between the tensile forces applied and the safety of closure of the incision. A parallel stainless steel 316L bar with an arrow at the end will indicate the level of forces applied based on the deformation in the arm of the hemostat. The CAD model can be seen in Figure 8.2 below.

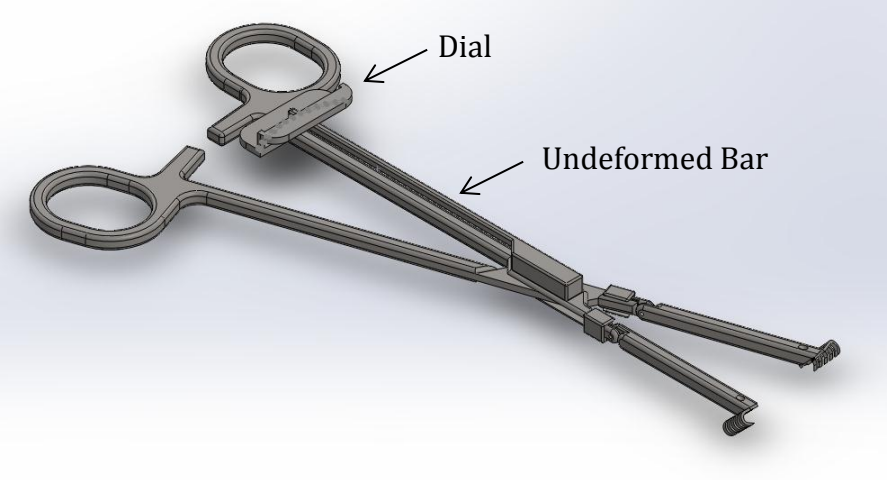

Figure 8.2: 3-D CAD Model of the Mechanical Device featuring the addition of the tensile force indicating ruler.

The procedural use would be the same as the final design iterated in Chapter 7. The device would be locked in the straightened position through the use of the locking collars during which the rakes would be attached to the deep fascia. As the surgeon applies the forces, the ratcheting mechanism is initiated and the deformation in the hemostat arm can start to be seen on the force indicator. With the prior knowledge of the individual patient's safe ranges from the provided chart, the surgeon will be able to complete the incision closure or deem the patient a candidate for gradual closure.

Additional long-term benefits for the mechanical design versus the electrical design include the marketability. Developing a device that is simple to use is predicted to enhance the desirability of the product for surgeons. Eliminating the electrical components would not only simplify the methods for sterilization but also reduce cost by increasing the longevity of the device's functionality. The purely mechanical workings would reduce the need for replacement parts and also increase the manufacturability of the device.

Ultimately the mechanical device has been designed to essentially replace the final design. The final design discussed previously was solely developed as a research tool, and once the necessary data has been collected, the mechanical device would be ideal to eliminate any electronics in the operating room. It is believed that the mechanical device would play a significant role in reducing the time spent closing incisions and decrease the occurrences of ventral hernias in patients undergoing a midline abdominal laparotomy.

Bibliography

Allied Electronics. (2013). *Nte electronics, inc. nte928m*. Retrieved from http://www.alliedelec.com/search/productdetail.aspx?SKU=70215846

Arduino (2013). *Wireless SD Shield.* Retrieved from http://arduino.cc/en/Main/ArduinoWirelessShield

Biswajit, Mohapatra (06/30/2004). "Staged abdominal repair (STAR) operation: How I did it". *Indian journal of surgery (0019-5650)*, 66 (3), p. 182.

Byeon, S. H., Kim, M., & Kwon, O. W. (2012). Ischemia. (pp. 23-49). Berlin, Heidelberg: Springer Berlin Heidelberg. doi: 10.1007/978-3-642-27410-7_2

Campbell, J.A, Temple, W.J., Frank, C.B., & Hutchcroft, S.A., (1989) A biomechanical study of suture pullout in linea alba. *Surgery* 106(5): 888-92. PMID:2530644

Ceydeli, A., Rucinski, J., & Wise, L.(2005) Finding the Best Abdominal Closure: An Evidence-based Review of the Literature. *Current Surgery.* 62(2), 220-225. doi:10.1016/j.cursur.2004.08.014

Ceydeli, A., Rucinski, J., & Wise, L.(2005) Finding the Best Abdominal Closure: An Evidence-based Review of the Literature. *Current Surgery.* 62(2), 220-225. doi:10.1016/j.cursur.2004.08.014

Clark J.L. (2001). Ventral incisional hernia recurrence. Journal of Surgical Research, 99(1), 33-33. doi: 10.1006/jsre.2001.6093

Cobb, W., Kercher, K., & Heniford, B. (2005). Laparoscopic repair of incisional hernias. *SURGICAL CLINICS OF NORTH AMERICA, 85*(1), 91-91.

Dermaclose®RC. Retrieved from http://www.dermaclose.com/

Digi (2013). *XBee 802.15.4 Device Connectivity Using Multipoint Wireless Networks.* Retrieved from http://www.digi.com/products/wireless-wired-embedded-solutions/zigbee-rf-modules/point-multipoint-rfmodules/xbee-series1-module.

Dunn MG, Silver FH. (1983) Viscoelastic behavior of human connective tissues: relative contribution of viscous and elastic components. *Connect Tissue*, 12:59–70.

Findley, Thomas, Chaudhry, Hans, Stecco, Antonio, Roman, Max. (2012). Fascia research: A narrative review**.** *Journal of Bodywork and Movement Therapie* 16 (1):67–75 http://dx.doi.org.ezproxy.wpi.edu/10.1016/j.jbmt.2011.09.004

Fox, J., & Tsoukas, M. M. (2010). A. vidimos, C. ammirati, C. poblete-lopez and D. elston, editors, requisites in dermatology: Dermatologic surgery, saunders elsevier ltd,

philadelphia, PA (2009), p. 261. *Clinics in Dermatology*, *28*(1), 110-111. doi: 10.1016/j.clindermatol.2009.10.002

Gallaudet, B.B. (2008) A description of the planes of fascia of the human body with special reference to the fascia of the abdomen, pelvis, and perineum. Copyright Triggerband LLC

Garfin, S. R., Tipton, C. M., Mubarak, S. J., Woo, S. L., Hargens, A. R., & Akeson, W. H. (1981). Role of fascia in maintenance of muscle tension and pressure. *Journal of Applied Physiology*,*51*(2), 317.

Haroon Javaid Majid, & Harun Majid Dar. (2011). Ventral Incisional Hernias. *The Professional Medical Journal*, *18*(2), 228-232.

Hope, W. W., Watson, L. I., Menon, R., Kotwall, C. A., & Clancy, T. V. (2010). Abdominal wall closure: Resident education and human error. *Hernia : The Journal of Hernias and Abdominal Wall Surgery*, *14*(5), 463-466.

Hutan, M (01/01/2010). "Sandwich Mesh Abdominal Closure". *Bratislavské lékarské listy (0006-9248)*, 111 (8), p. 461.

Kaplan, M (10/01/2005). "Guidelines for the management of the open abdomen". *Wounds (King of Prussia, Pa.) (1044-7946)*, p. 1.

Kenedi, R.M., Gibson, T., Evans, J.H., & Barbenel, J.C. (1975) Tissue Mechanics. *Phys. Med. Biol.* 20 (5): 699-717. http://iopscience.iop.org.ezproxy.wpi.edu/0031-9155/20/5/001/pdf/0031-9155_20_5_001.pdf

Kirilovam M., Stoytchev, S., Pashkouleva, D.,&Kavardzhikov, V. (2011). Experimental study of the mechanical properties of human abdominal fascia. *Medical Engineering & Physics.* 33:1-6.

Kirilovam M., Stoytchev, S., Pashkouleva, D., Tsenova, V., &Kristoskova, R. (2009) Viscoelastic mechanical properties of the human abdominal fascia. *Journal of Bodywork & Movement Therapies.*13: 336-337.

Laparotomy, exploratory. (2007). *Encylopedia of Surgery*(5th ed.). Advameg, Inc. http://www.surgeryencyclopedia.com/La-Pa/Laparotomy-Exploratory.html

Lim, C.T. and Goh, J.C.H. (2010). IFMBE Proceedings 31:1000–1003.

Lineaweaver, W. (2012). Improvement of success rates for abdominal component reconstructions using bovine fetal collagen. *Annals of Plastic Surgery, 68*(5), 438-441.

Madison, K. C. (2003). Barrier function of the skin: "la raison d'être" of the epidermis.

Journal of Investigative Dermatology, *121*(2), 231-241. doi:10.1046/j.1523-1747.2003.12359.x

McCracken, Thomas (2000). *New Atlas of Human Anatomy.* China: Metro Books. 1-240. ISBN 1-58663-097-0.

Mouser Electronics. (2013). *Arduino UNO Microcontroller Board.* Retrieved from http://www.mouser.com/new/arduino/arduinouno/?cm_mmc=google-_-ppc-_-americas-_-Arduino&gclid=CP7AtNuj1LUCFfBDMgodxnoADw

Navsaria, P. H., Bunting, M., Omoshoro-Jones, J., Nicol, A. J. and Kahn, D. (2003), Temporary closure of open abdominal wounds by the modified sandwich–vacuum pack technique. Br J Surg, 90: 718–722. doi: 10.1002/bjs.4101

Park, A. E., Roth, J. S., & Kavic, S. M. (2006). Abdominal wall hernia. *Current Problems in Surgery*, *43*(5), 326-375. doi: 10.1067/j.cpsurg.2006.02.004

Pfannenstiel, H. J. (1990). Ueber die Vortheile des suprasymphysären Fascienquerschnitts für die gynäkologischen Koeliotomien. *Sammlung klinischer Vorträge* 267(97):1735-1756.

Proksch, E., Brandner, J. M., & Jensen, J. (2008). The skin: An indispensable barrier. *Experimental Dermatology*, *17*(12), 1063-1072. doi:10.1111/j.1600-0625.2008.00786.x

Schachtrupp, A., Fackeldey, V., Klinge, U., Hoer, J., Tittel, A., Toens, C., & Schumpelick, V. (2002). Temporary closure of the abdominal wall (laparostomy). *Hernia*, *6*, 155-162.

Silver, F. H., Freeman, J. W., & DeVore, D. (2001). Viscoelastic properties of human skin and processed dermis. *Skin Research and Technology : Official Journal of International Society for Bioengineering and the Skin (ISBS) [and] International Society for Digital Imaging of Skin (ISDIS) [and] International Society for Skin Imaging (ISSI), 7*(1), 18-23. doi:10.1034/j.1600-0846.2001.007001018.x

Standring, Susan PhD DSc (2008). *Gray's anatomy*. (39 ed.). Elsevier Inc.

Silver FH, Kato YP, Ohno M, Wasserman AJ. (1992) Analysis of mammalian connective tissue: relationship between hierarchical structures and mechanical properties. *J Long-term Effect Med Implants* 2:165–198.

Song, A., Askaro, M., Azemi., Alber., Hurwitz.,D., Marra, K., Shestak, K., Debski., & Rubin, P. (2004). Biomechanical Properties of the Superficial Fascial System. *The Aesthetic Meeting 2004 of the American Society for Aesthetic Plastic Surgery (ASAPS).* The American Society for Aesthetic Plastic Surgery, Inc. doi:10.1016/j.asj.2006.05.005

Stecco, Carla. (2011). "The fascia: the forgotten structure". Italian journal of anatomy and embryology. 116(3):127.

Stein, D. E., MD. Intestinal fistulas. *Medscape*, Retrieved from http://emedicine.medscape.com/article/179444-clinical

Stremitzer, S. (09/01/2004). "Prospective evaluation of vacuum-assisted fascial closure after open abdomen: planned ventral hernia rate is substantially reduced". *European surgery (1682-8631)*, 36 (4), p. 266.

Stücker, M., Struk, A., Altmeyer, P., Herde, M., Baumgärtl, H., & Lübbers, D. W. (2002). The cutaneous uptake of atmospheric oxygen contributes significantly to the oxygen supply of human dermis and epidermis. *The Journal of Physiology, 538*(3), 985-994. doi:10.1113/jphysiol.2001.013067

Sukumar, N (06/01/2004). "Bogota bag in the treatment of abdominal wound dehiscence". *Medical journal of Malaysia (0300-5283)*, 59 (2), p. 281.

van Ramshorst, G. H., Eker, H. H., Hop, W. C. J., Jeekel, J., & Lange, J. F. (2012). Impact of incisional hernia on health-related quality of life and body image: A prospective cohort study. *American Journal of Surgery, 204*(2), 144-150. doi: 10.1016/j.amjsurg.2012.01.012

Vishay Precision Group. Micro-Measurements: Strain Gages and Instruments: Application Note TT-612.

Vishay Precision Group. Micro-Measurements: Strain Gages and Instruments: Tech Note TN-505-4.

Weisman, S. (2006). U.S. Patent No. 7,478,563. Toronto, Ontario, CA: U.S. Patent and Trademark Office.

Appendices

Appendix A: Objectives Tree

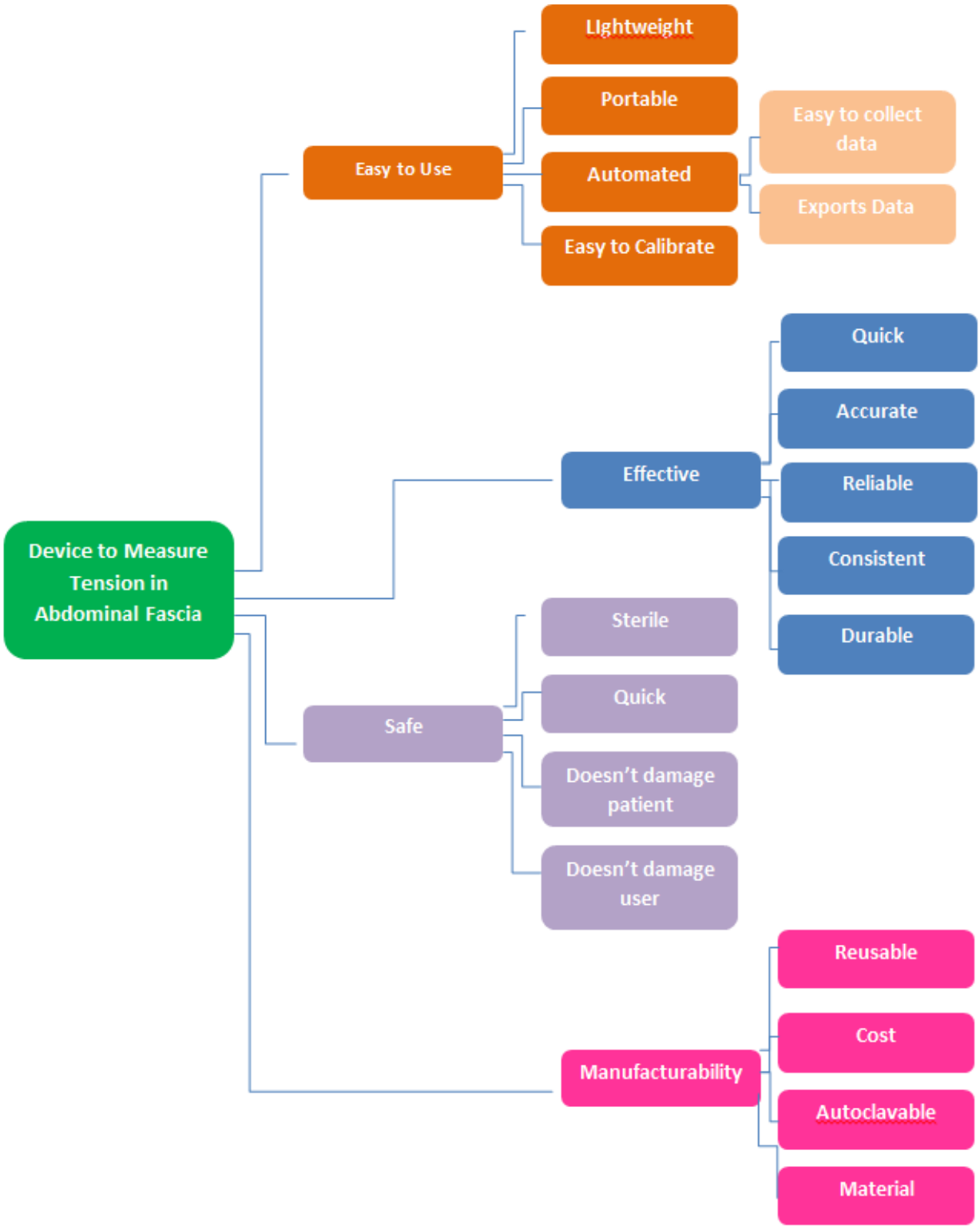

Appendix B: Pairwise Comparison Chart completed by Dr. Raymond Dunn

	Easy to Use	Effective	Safe	Manufacturability	Totals
Easy to Use		0	0	0	0
Effective	1		0	0	1
Safe	1	1		1	3
Manufacturability	1	1	0		2

Easy to Use Pairwise Comparison

	Lightweight	Portable	Automated	Easy to Cailbrate	Totals
Lightweight		0.5	0.5	0.5	1.5
Portable	0.5		1	0.5	2
Automated	0.5	0		0.5	1
Easy to Calibrate	0.5	0.5	0.5		1.5

Effective Pairwise Comparison

	Quick	Accurate	Reliable	Consistent	Durable	Totals
Quick		0	0	0	0	0
Accurate	1		0.5	0.5	1	3
Reliable	1	0.5		0.5	1	3
Consistent	1	0.5	0.5		1	3
Durable	1	0	0	0		1

Safe Pairwiase Comparison

	Sterilzable	Quick	Safe Patient	Safe User	Totals
Sterilizable		1	0.5	0.5	2
Quick	0		0	0	0
Safe Patient	0.5	1		0.5	2
Safe User	0.5	1	0.5		2

Manufacturability Pairwise Comparison

	Reusable	Cost	Sterilizable	Totals
Reusable		0.5	0.5	1
Cost	0.5		0.5	1
Sterilizable	0.5	0.5		1

Appendix C: Pairwise Comparison Completed by Team

Overall Objectives Pairwise Comparison

	Easy to Use	Effective	Safe	Manufacturability	Totals
Easy to Use		0	0	1	1
Effective	1		0	1	2
Safe	1	1		1	3
Manufacturability	0	0	0		0

Easy to Use Pairwise Comparison

	Lightweight	Portable	Automated	Easy to Cailbrate	Totals
Lightweight		0.5	1	0	1.5
Portable	0.5		1	0	1.5
Automated	0	0		0	0
Easy to Calibrate	1	1	1		3

Effective Pairwise Comparison

	Quick	Accurate	Reliable	Consistent	Durable	Totals
Quick		0	0	0	0	0
Accurate	1		0.5	0.5	1	3
Reliable	1	0.5		0.5	1	3
Consistent	1	0.5	0.5		1	3
Durable	1	0	0	0		1

Safe Pairwiase Comparison

	Sterilzable	Quick	Safe Patient	Safe User	Totals
Sterilizable		1	0.5	0.5	2
Quick	0		0	0	0
Safe Patient	0.5	1		0.5	2
Safe User	0.5	1	0.5		2

Manufacturability Pairwise Comparisor

	Reusable	Cost	Sterilizable	Manufacturability	Totals
Reusable		0.5	0	1	1.5
Cost	0.5		0	1	1.5
Sterilizable	1	1		1	3
Material Quailty	0	0	0		0

Appendix D: Pairwise Comparison Chart with Combined Scores

Overall Objectives Pairwise Comparison

	Easy to Use	Effective	Safe	Manufacturability	Totals
Easy to Use		0	0	0.5	0.5
Effective	1		0	0.5	1.5
Safe	1	1		1	3
Manufacturability	0.5	0.5	0		1

Easy to Use Pairwise Comparison

	Lightweight	Portable	Automated	Easy to Cailbrate	Total
Lightweight		0.5	0.75	0.25	1.5
Portable	0.5		1	0.25	1.75
Automated	0.25	0		0.25	0.5
Easy to Calibrate	0.75	0.75	0.75		2.25

Effective Pairwise Comparison

	Quick	Accurate	Reliable	Consistent	Durable	Totals
Quick		0	0	0	0	0
Accurate	1		0.5	0.5	1	3
Reliable	1	0.5		0.5	1	3
Consistent	1	0.5	0.5		1	3
Durable	1	0	0	0		1

Safe Pairwiase Comparison

	Sterile	Quick	Safe Patient	Safe User	Totals
Sterile		1	0.5	0.5	2
Quick	0		0	0	0
Safe Patient	0.5	1		0.5	2
Safe User	0.5	1	0.5		2

Manufacturability Pairwise Comparison

	Reusable	Cost	Sterilizable	Material Quality	Totals
Reusable		0.5	0.25	1	1.75
Cost	0.5		0.25	1	1.75
Sterilizable	0.75	0.75		0	1.5
Material Quality	0	0	0		0

Appendix E: Spider with Torque Sensor & Spider with Strain Gage

The first two design alternatives were very similar. The body and the application of the device were the same, only varying with the method for applying tensile forces. Known as the “Spider”, the device consisted of a main body that would be positioned directly above the open wound with cable attachments that extended from both sides to attach to the fascia. Tensile forces would be applied via a drill acting as rotary motor with a torque wrench, and measurements would be recorded through a torque sensor, or with the use of fish scale weights, both shown in the figures below.

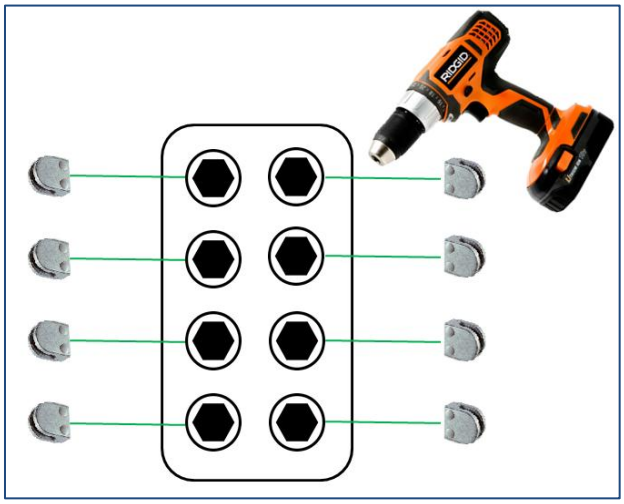

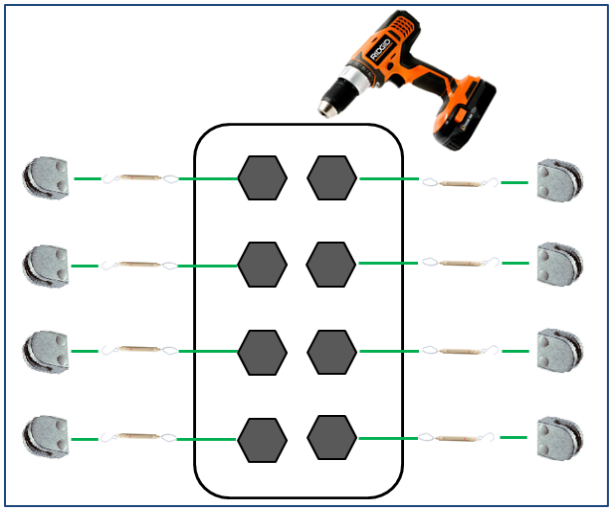

A clamp similar to a surgical towel clamp would hold both the fascia and skin layers of the abdominal wall. The other end of the towel clamp would be attached to a nylon cable that would lead to the internal ratchet found at the other end. The internal components of the device are

comprised of the dual rows of ratchets that run the length of the device body. For each cable and attachment clamp, there is a ratchet on the same side from which the cable would extrude. A rotary motor (the power drill) attached to the ratchet would wind the cable around the internal crank, applying tensile forces at points along the fascia. The drill would have a specially designed hex head to fit the bit and the ratchet would aid in locking the cable into place when the drill stopped winding the cable in.

For Design 1, the torque measurements (Nm) would be recorded using a torque sensor, and data would be exported to for further analysis. Separate data would be collected for each ratchet. Design 2 has the same exporting approach, but individual tensile force measurements would be taken by fish scale weights attached to each cable.

Appendix F: Half Spider Design 1: Cranking Mechanism or Small Motors

Design 3 and 4 were variations of the previous design, the "Spider". These two designs can be described by symmetrically dividing the spider vertically down the center. The device body would contain only one row of ratchets with the connected cable and clamp.

The main difference would be the positioning and method of use of the device. The procedure would call for two separate "Half Spider" devices, with one located on each side of the patient. Both devices would be positioned level with the open wound, and clamps would be attached to the opposite side of wound. To avoid intertwining the cables, they would be carefully positioned to alternate. The single device with the torque sensor and the fish scale weight version can be seen in the two figures below.

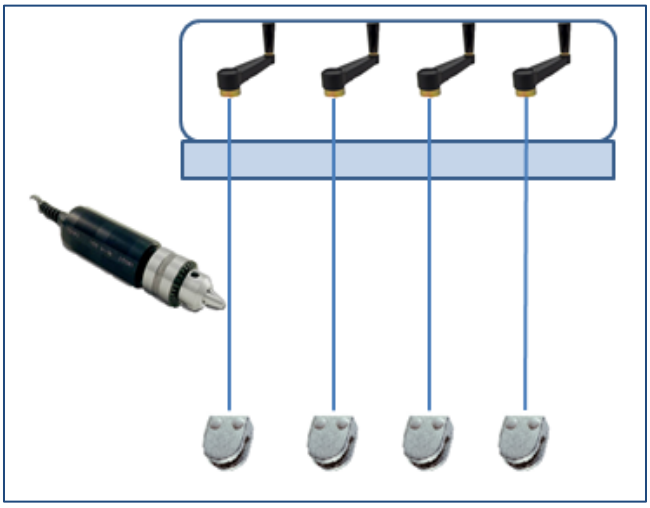

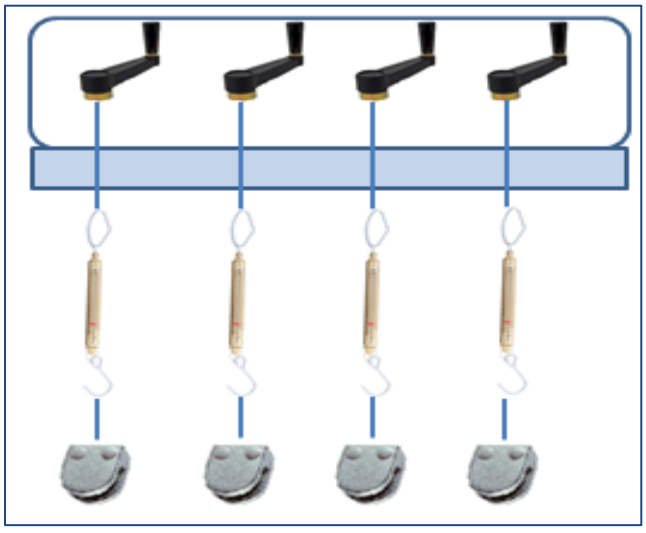

The same clamp attachment from the spider will be used for the “Half Spider” device to grip the fascia and dermal layers. The cables would be attached to the clamp and the internal ratchet. A hand crank would be used to wind the cable around the ratchet. The ability to lock the cable when the ratchet is not being wound would be necessary for the crank to maintain the tensile force being applied.

Design 3 and 4 vary by their means of tensile force measurements. Design 3 uses the torque sensor at the head of the crank to measure the forces being applied. These values would be exported for analysis. Design 4 would use the fish scale weights attached to each cable to measure the tensile forces from the device, and measurements would be exported.

Appendix G: FasciaClose

The concept behind the FasciaClose (original sketches found in Appendix F) is a frictionless pulley system that laces through the wound in order to apply and measure the tensile forces. The device is a variation of the DermaClose, a readily available closure device used for gradual wound closure. The Figure below is a representation of the FasciaClose system showing the clamps with the pulleys, the lacing cable, and the device with the crank and fish scale weights.

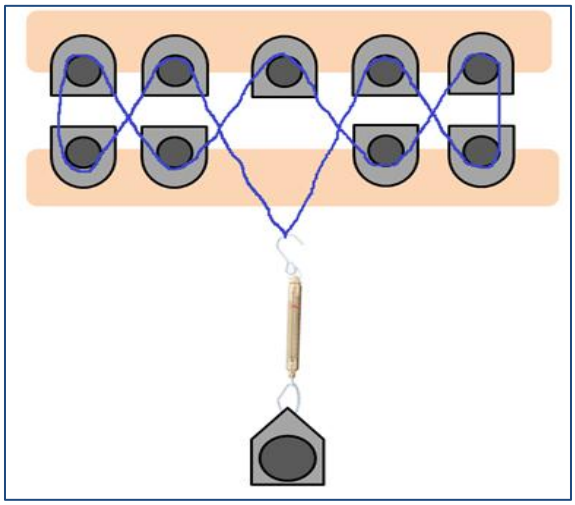

A surgical towel clamp, mentioned previously, would be used for attachment to the fascial and dermal layers. Cable would be fed through a pulley located on the top portion of each clamp and would form one large loop, ending in the cranking mechanism of the device. The main body of the device would hold the crank and ratchet that is used to apply the tensile force. The knob of the crank would be wound continuously applying the desired force to the cable. As the cable tightens throughout the pulley system drawing the fascia closed, the strain gage connected to the cable will read the measurements that are being taken during the procedure and would be exported.

Appendix H: Dual Retractor

This design consists of dual retracting clamps with a fish scale weight in the center. Ends of the device would be attached via a surgical towel clamp and pulled towards each other initiating a force on the fascia and skin layers. The strain gage would read the measured tensile force and export data for analysis.

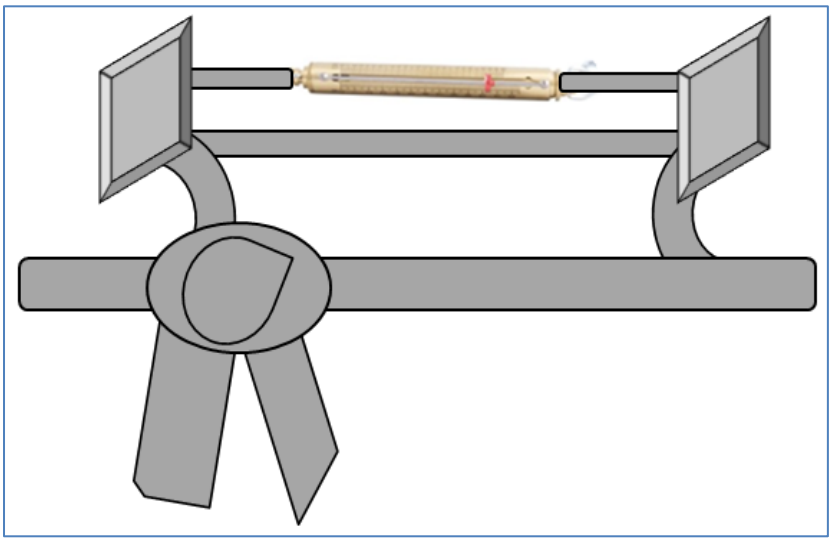

Appendix I: Retracting Ribs Design One: Multiple Cranks or Master Crank

Designed to mimic the similarity of the human rib cage, this device would consist of a stationary center bar running vertically over the wound and small horizontal bars extending to the sides of the wound. At the end of these horizontal extensions would be surgical towel clamps to attach to the fascia and dermal layers. At the intersection of the bars with the center anchor, there would be an elevated crank. Once attached, the device would apply tensile forces by turning the crank at each location. When the crank is turned, the horizontal bars would slide through each other in the allotted space beneath the crank applying a constant force on the abdominal wall. A force transducer located on each clamp would measure tensile forces and export data for further analysis.

A variation of the retracting ribs design would limit the number of elevated cranks to one centrally located along the stationary vertical bar. The crank, when turned, would pull all of the horizontal extensions toward the center bar, simultaneously applying tensile forces along the entire length of the wound on both sides, offering a simplified and quicker measurement process. Located at the central crank would be a force transducer taking tensile force measurements corresponding to the forces in the abdominal over the entire incision. Data would be exported for further analysis. The sketches for these two designs can be seen below.

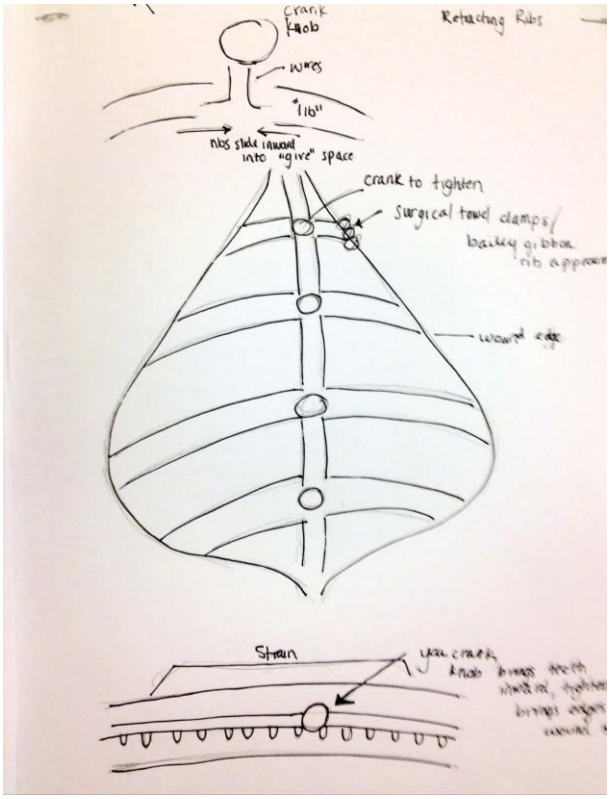
Retaining Ribs
crank knob
wires
"rib"
ribs slide inward into "give" space
crank to tighten
Surgical towel clamps/
wound edge
Strain

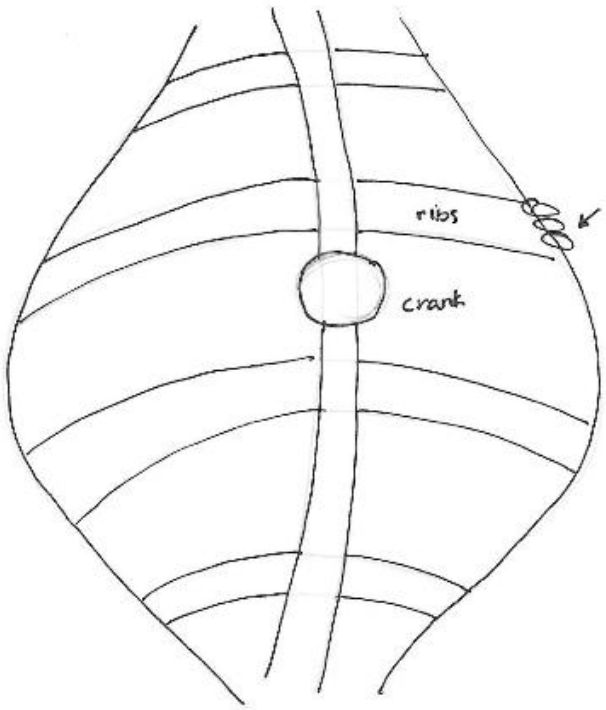
ribs
crank

L

Appendix J: Tissue Plates

Shown in the sketch below, this device consists of an elongated stainless steel plate with large perforated holes spaced along its length. The plate would be aligned along the length of the incision, and at each hole, a suture would be passed through the abdominal tissue and the hole, effectively tying the plate to the abdominal fascia at various points. Bonded to the plate at its midpoint would be a force transducer. Plates are located along both sides of the incision and pulled toward the linea alba, which would cause the tissue to experience an applied force. The tensile forces would be numerically translated into data by the force transducer and output to a nearby computer. Plate size could be varied to accommodate a range of incision sizes, offering a moderate level of flexibility.

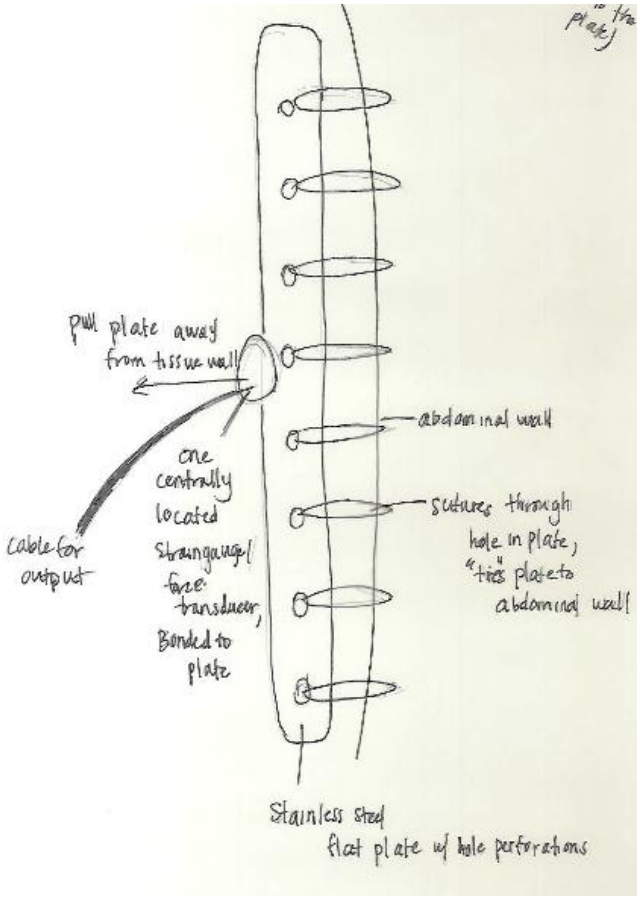

Appendix K: Initial Weighted Function Means Charts

The next step was to compare the options based on the ranking of the objectives. Using the Pairwise Comparison Chart completed by Dr. Raymond Dunn and the Team PCC, a final PCC was created using the average rankings. These final ranks were used to determine the importance of each objective and weight it accordingly. Then the team individually scored the designs based on the objectives, and finalized the average scores by multiplying by objective weight. These evaluations led to the selection of the final design. The first weighted function-means chart in showed that FasciaClose would best meet the design objectives and constraints based upon its highest overall score of 84%.

The FasciaClose design would give data that corresponds to one overall tensile force measurement in the abdominal wall during the closure of midline abdominal laparotomy incisions. It would attach via specialized surgical towel clamps, and collect data using a fish scale weight located at the cranking portion of the device.

Design Constraints		Spider (Torque)	Spider (Strain Gauge)	Half Spider (Torque)	Half Spider (Strain Gauge)	Fasciaclose	Clamps
Cannot exceed $950		N	Y	N	Y	Y	Y
IRB/IACUC		Y	Y	Y	Y	Y	Y
Patient Consent		Y	Y	Y	Y	Y	Y
FDA Regulations		Y	Y	Y	Y	Y	Y
Sterile		Y	Y	Y	Y	Y	Y

Design Objectives		Spider (Torque)		Spider (Strain Gauge)		Half Spider (Torque)		Half Spider (Strain Gauge)		Fasciaclose		Clamps	
	Weight	Score	Weighted Score	Score	Weighted Score	Score	Weighted Score	Score	Weighted Score	Score	Weighted Score	Score	Weighted Score
Easy to Use	0.08	0.20	0.02	0.10	0.01	0.40	0.03	0.10	0.01	0.90	0.07	0.60	0.05
Effective	0.25	0.80	0.20	0.67	0.17	0.83	0.21	0.60	0.15	0.89	0.22	0.20	0.05
Safe	0.50	0.77	0.38	0.53	0.27	0.60	0.30	0.33	0.17	0.82	0.41	0.85	0.43
Manufacturability	0.17	0.10	0.02	0.10	0.02	0.10	0.02	0.05	0.01	0.78	0.13	0.90	0.15
Total	100.00		0.62		0.46		0.56		0.33		0.84		0.68

N

Appendix L: Final Selection Matrix

Design Objectives		Instrumented Kelley Forceps		Instrumented Blunt Nose Forceps		Spatula Forceps		Tissue Plates		Multiple Cranks & Ribs		Master Crank & Ribs		Single Spring & Transducer	
	Weight	Score	Weighted Score	Score	Weighted Score	Score	Weighted Score	Score	Weighted Score	Score	Weighted Score	Score	Weighted Score	Score	Weighted Score
Easy to Use	0.80	9	7.2	9	7.2	9	7.2	6	4.8	4	3.2	5	4	10	8
Effective	2.50	6	15	3	7.5	2	5	4	10	4	10	5	12.5	2	5
Safe	5.00	7	35	7	35	7	35	2	10	4	20	4	20	8	40
Manufacturability	1.70	10	17	10	17	10	17	10	17	4	6.8	5	8.5	9	15.3
Total	10.00	32	74.2	29	66.7	28	64.2	22	41.8	16	40	19	45	29	68.3

Design Objectives		Multiple Springs & Transducers		L Clamp		Curved Forceps		Elevated Retractor Forceps		Disengaging Forceps	
	Weight	Score	Weighted Score	Score	Weighted Score	Score	Weighted Score	Score	Weighted Score	Score	Weighted Score
Easy to Use	0.80	4	3.2	9	7.2	9	7.2	10	8	9	7.2
Effective	2.50	4	10	6	15	4	10	7	17.5	9	22.5
Safe	5.00	4	20	4	20	4	20	9	45	9	45
Manufacturability	1.70	4	6.8	8	13.6	9	15.3	10	17	10	17
Total	10.00	16	40	27	55.8	26	52.5	36	87.5	37	91.7

Appendix M: Strain Gage Detailed Description

For the selection of the strain gage, the strain-sensing alloy was selected to be Constantan. Of all alloys used, Constantan is the oldest and remains the most frequently used. This is because it is considered to have the ideal overall composition of characteristics necessary for a wide range of applications. These characteristics include a high gage factor which directly correlates to the strain sensitivity. This means that a gage made out of Constantan is insensitive to strain level and temperature, which was an important aspect of the forceps because of the necessary repetitive sterilization through autoclaving at excessive temperatures. Its resistivity is also high enough that it can achieve resistance values in very small grids. Constantan has also been noted to have high cyclic endurance (Vishay, TN-505-4).

The backing material was selected from the two commonly used polyimide and glass-fiber-reinforced epoxy-phenolic. The polyimide backing was selected because of its extremely flexible characteristics. This material can be contoured readily to accommodate small radii. The high peel strength of the polyimide makes the gage less apt to mechanical damage during installation. It is able to be used in a wide temperature range of -320° to +350°F and is capable of large elongations (Vishay, TN-505-4).

In order to accommodate the standard size of forceps, the gage with the smallest length and width available in the materials noted above was selected. Therefore, of the available gages, the gage length was determined to be 0.38mm. The overall length is 3.56mm, while the overall width is 2.67mm. Therefore, the thickness of the forceps model was modeled to accommodate the strain gage, with a total thickness of 6.35mm. With those selections, the available gage had a resistance of 120 ±3% (Vishay, TN-505-4).

Appendix N: Autoclavable and Wireless Strain Gage Circuit Description

The complete circuit, which can be seen in the Figure below, involves six major components that together collect and amplify voltages generated by the strain gage, convert signals from analog to digital, and then store and transmit this data for analysis. The strain gage is incorporated into a ¼ bridge Wheatstone configuration, and generated voltages are transmitted to an operational amplifier (Op Amp) where they are magnified according to determined settings. Amplifying the voltages allows the microcontroller (MC) to read these signals. An essential component of the MC is the analog to digital (A/D) converter, where voltages are converted from binary sequences to digital values. These values move from the A/D converter to the XBee Digi Module (XBee), which links the wireless shield to the circuit. Data is stored as flash memory in an SD card located on the Wireless Shield as well as transmitted via radio frequencies to a receiver for later analysis. The entire circuit is powered by a lithium ion battery (V).

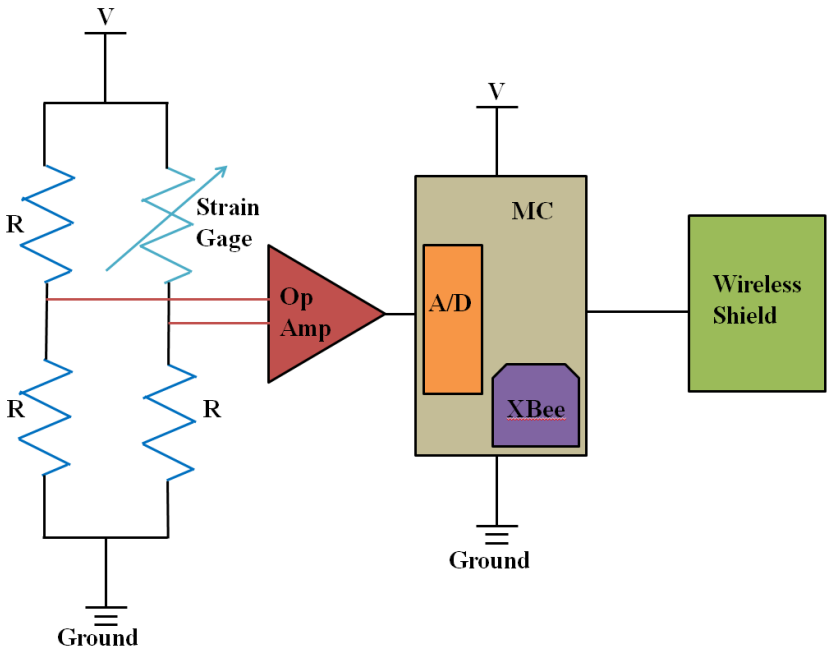

The Wheatstone bridge consists of a strain gage and three reference resistors, selected to keep the bridge balanced and generate no voltage when the hemostats are not in use. As the hemostats are applied, the stainless steel deforms due to the tensile forces in the deep fascia, generating voltages across the Wheatstone bridge. These voltages travel to an Op Amp, specifically the NTE Electronics IC-Dual Low Power Op Amp, seen in the next Figure. This Op Amp allows an amplification of 100V/mV and requires a low voltage supply of 5V (Allied Electronics, 2013).

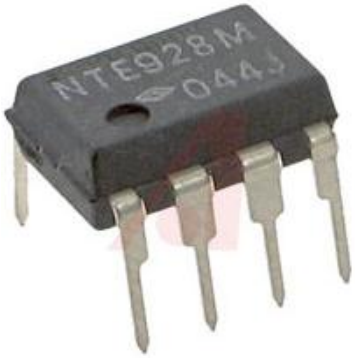

Voltages then travel to a MC, such as the Arduino UNO Microcontroller seen in the following Figure. The Arduino microcontroller development board consists of 14 digital inputs and outputs and 6 analog outputs, and can be powered by a USB connection or a power source of 5V (Mouser, 2013). Included in the Arduino UNO is a USB to serial convertor, which converts generated voltages from analog to digital values.

Stacked onto the Arduino UNO Microcontroller is Digi's XBee 802.15.4 Module, as shown in the Figure below. The XBee Module allows for easy communication over radio frequencies (RF) at a rate of up to 250 kilobytes per second (kbps) (Digi, 2013). Features such as sleep modes for extended battery life and pre-programmed controls that facilitate immediate and easy connection with the Arduino Wireless SD Shield seen in Figure 44, make Digi's XBee 802.15.4 Module an optimal fit for this circuit.

R

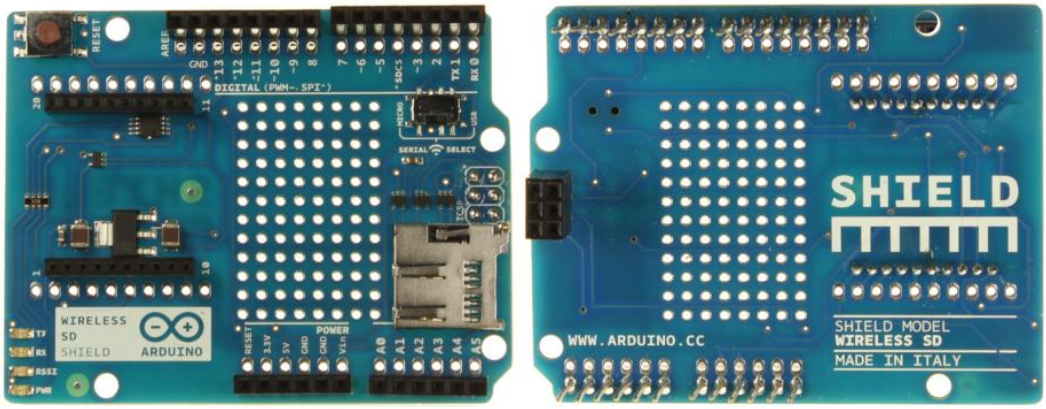

The Wireless SD Shield from Arduino is designed to communicate with the XBee 802.15.4 Module, and has a range up to 100 ft. (Arduino, 2013). In addition to wirelessly transmitting the data, it is equipped with a SD slot for flash memory, allowing a hard copy to be written and stored as data is collected (Arduino, 2013). A critical component of the Wireless SD Shield is the on-board switch which enables the shield to wirelessly communicate with the Arduino UNO Microcontroller and the USB to serial converter (Arduino, 2013).

Appendix O: MATLAB Scripts

```
%%Instron Material Testing
%Stainless Steel 316L

%%Specimen One Dimensions

%Notes: Segment is slightly curved, rounded in shape, cut from the arm of a
%pair of pre-existing forceps

l=4.58; %segment length in mm
L=52.4; %distance between spacers in mm
d=118; %segment diameter in mm
r=d/2; %segment radius in mm
A=pi*r^2 %cross sectional area of the segment in mm^2
I=(pi*(r^4))/4 %Moment of Inertia in mm^4

%%Importing Data
fileName='Metal_One.csv';
data=dlmread(fileName,',',7,0);

T=data(:,1); %Time(sec)
u1=(data(:,2)); %Extension (mm)
f1=(data(:,3)); %Force applied (N)
U=-1*u1;
F=-1*f1;


%% Calculations

stress=F/A; %stress in N/mm^2
strain=(L+U)/L; %strain
x=stress;
y=strain;

%% Plots

%Load versus Deflection
figure(1)
plot(F,U)
xlabel('Load Applied (N)'); ylabel ('Displacement (mm)'); title ('Load Applied versus
Displacement (SS316L Specimen One)');

%%POLYFIT
%% Fit: 'Specimen1_PF'.
[xData, yData] = prepareCurveData( F, U );

% Set up fittype and options.
ft = fittype( 'poly2' );
opts = fitoptions( ft );
opts.Lower = [-Inf -Inf -Inf];
opts.Upper = [Inf Inf Inf];

% Fit model to data.
[fitresult, gof] = fit( xData, yData, ft, opts );

% Plot fit with data.
```

```
figure( 'Name', 'Specimen1_PF' );
h = plot( fitresult, xData, yData);
legend( h, 'Actual Data', 'Fit', 'Location', 'NorthEast' );
% Label axes
xlabel( 'Applied Force (N)' );
ylabel( 'Deflection (mm)' );
grid on
title('Polynomial Fit for SS316L Specimen 2: Deflection vs. Applied Force');

%%RATIONAL FIT
%% Fit: 'Specimen1_RF1'.
[xData, yData] = prepareCurveData( F, U );

% Set up fittype and options.
ft = fittype( 'rat21' );
opts = fitoptions( ft );
opts.Display = 'Off';
opts.Lower = [-Inf -Inf -Inf -Inf];
opts.StartPoint = [0.748151592823709 0.450541598502498 0.0838213779969326
0.228976968716819];
opts.Upper = [Inf Inf Inf Inf];

% Fit model to data.
[fitresult, gof] = fit( xData, yData, ft, opts );

% Plot fit with data.
figure( 'Name', 'Specimen1_RF1' );
h = plot( fitresult, xData, yData);
legend( h, 'Acutal Data', 'Fit', 'Location', 'NorthEast' );
% Label axes
xlabel( 'Applied Force (N)' );
ylabel( 'Deflection (mm)' );
grid on
title ('Rational Fit for SS316L Specimen 2: Deflection vs. Applied Force');

%%Instron Material Testing
%Stainless Steel 316L

%%Specimen Two

%Notes: Segment is slightly curved, rounded in shape, cut from the arm of a
%pair of pre-existing forceps

l=4.78; %segment length in mm
L=52.4; %distance between spacers in mm
d=119; %segment diameter in mm
r=d/2; %segment radius in mm
A=pi*r^2 %cross sectional area of the segment in mm^2
I=(pi*(r^4))/4 %Moment of Inertia in mm^4

%%Importing Data
fileName='MetalTwo.csv';
data=dlmread(fileName,',',7,0);

T=data(:,1); %Time(sec)
u2=(data(:,2)); %Extension (mm)
f2=(data(:,3)); %Force applied (N)
U=-1*u2;
F=-1*f2;
```

U

```
%% Calculations

stress=F/A; %stress in N/mm^2
strain=(L+U)/L; %strain
x=stress;
y=strain;

%% Plots

%Load versus Deflection
figure(1)
plot(F,U)
xlabel('Load Applied (N)'); ylabel ('Displacement (mm)'); title ('Load Applied versus
Displacement (SS316L Specimen Two)');

%%RATIONAL FIT
%% Fit: 'Specimen2RF'.
[xData, yData] = prepareCurveData( F, U );

% Set up fittype and options.
ft = fittype( 'rat21' );
opts = fitoptions( ft );
opts.Display = 'Off';
opts.Lower = [-Inf -Inf -Inf -Inf];
opts.StartPoint = [0.825816977489547 0.538342435260057 0.996134716626885
0.0781755287531837];
opts.Upper = [Inf Inf Inf Inf];

% Fit model to data.
[fitresult, gof] = fit( xData, yData, ft, opts );

% Plot fit with data.
figure( 'Name', 'Specimen2RF' );
h = plot(fitresult,xData,yData);
legend( h, 'Actual Data', 'Fit', 'Location', 'NorthEast' );
% Label axes
xlabel( 'Applied Force (N)' );
ylabel( 'Deflection (mm)' );
grid on
title ('Rational Fit for SS316L Specimen 1: Deflection vs. Applied Force');

%%POLYFIT
%% Fit: 'Specimen2PF'.
[xData, yData] = prepareCurveData( F, U );

% Set up fittype and options.
ft = fittype( 'poly2' );
opts = fitoptions( ft );
opts.Lower = [-Inf -Inf -Inf];
opts.Upper = [Inf Inf Inf];

% Fit model to data.
[fitresult, gof] = fit( xData, yData, ft, opts );

% Plot fit with data.
figure( 'Name', 'Specimen2PF' );
```

```
h = plot( fitresult, xData, yData );
legend( h, 'Actual Data', 'Fit', 'Location', 'NorthEast' );
% Label axes
xlabel( 'Applied Force (N)' );
ylabel( 'Deflection (mm)' );
grid on
title('Polynomial Fit for SS316L Specimen 1: Deflection vs. Applied Force');
```

W

Appendix P: Radius of Curvature Calculations (Mechanical Testing)

In order to determine deflection and radius of curvature, three-point bending tests using an Instron mechanical testing machine were performed on two specimens of stainless steel 316L. Both specimens were cut from the arms of a pair of 12-inch hemostats using a hacksaw and filed to eliminate sharp edges. It is important to note that both specimens were slightly curved along their length. Collected data was analyzed using MATLAB, and the data was fit using the curve-fitting tool. The MATLAB scripts, graphs, and equations of fit used for analysis can be found in Appendix O. The optimal fit was selected based on Sum Square of Errors (SSE), coefficient of determination (R^2), and Root Mean Squared Error (RMSE) values.

By using the polynomial fits for specimens one and two, a curve was established relating deflection (mm) of the SS316L to the applied force (N). Using these models, the deflection of SS316L can be determined for the load of 116.4N, the maximum amount of force that will be applied using the retaining forceps. The deflection from the force allows for the calculation of the radius of curvature of the SS316L for its use as a material for the retaining forceps. Radius of curvature calculations can be seen in full in Appendix DD. For a load of 116.4N: it will deflect by $2.217*10^{-4}$m according to the polynomial equation from specimen one; and it will deflect by $1.704*10^{-4}$m according to the polynomial equation from specimen two. The calculated stress on the cross sectional area of the forceps due to the force of the fascia is $1.442*10^{6}$ N/m^2, and the Young's Modulus of stainless steel 316L is 190GPa. Substituting these values into the formula seen below, the radius of curvature was able to be calculated for both specimens.

$$Radius\ of\ Curvature = \frac{(Young's\ Modulus * Deflection)}{(Stress)}$$

This equation showed that the radius of curvature, according to specimen one and specimen two values for deflection, would be 29.189m and 22.429m, respectively. This large radius indicates that the forceps would not bend significantly when loaded with the 116N of force due to the fascia.

Based upon the results of the analytical calculations and the mechanical testing to determine radius of curvature, it was able to be concluded that the stainless steel hemostats would experience a great enough deflection that the strain gage would be able to detect strains due to loading. It is important to note that the hemostats are a complex geometry, and that the previously mentioned calculations are not accurate to that specific geometry.

Radius of Curvature Calculations

$E := 190 \cdot 10^{9} \ \frac{N}{m^2}$

$t := 1.27 \ cm$

$w := 0.635 \ cm$

$Across := t \cdot w \quad Across = (8.065 \cdot 10^{-5}) \ m^2$

$Ffascia := 116.4 \ N$

$\sigma := \frac{Ffascia}{Across} \quad \sigma = (1.443 \cdot 10^{6}) \ \frac{N}{m^2}$

$yspecimen1 := (-2.097 \cdot 10^{-8} \ mm) \cdot 116.4^2 + (0.00111 \ mm \cdot 116.4) + 0.09282 \ mm$

$yspecimen1 = (2.217 \cdot 10^{-4}) \ m$

$yspecimen2 := (1.121 \cdot 10^{-7} \ mm) \cdot 116.4^2 + (0.0008498 \ mm \cdot 116.4) + 0.06995 \ mm$

$yspecimen2 = (1.704 \cdot 10^{-4}) \ m$

$R1 := \frac{(E \cdot yspecimen1)}{\sigma} \quad R1 = 29.189 \ m$

$R2 := \frac{(E \cdot yspecimen2)}{\sigma} \quad R2 = 22.429 \ m$

Y